Development/Plasticity/Repair

MicroRNA-9 Regulates Neurogenesis in Mouse Telencephalon by Targeting Multiple Transcription Factors

Mikihito Shibata,[1] Hiromi Nakao,[1] Hiroshi Kiyonari,[2] Takaya Abe,[2] and Shinichi Aizawa[1,2]

Laboratories for [1]Vertebrate Body Plan and [2]Animal Resources and Genetic Engineering, Center for Developmental Biology, RIKEN Kobe, Chuo-ku, Kobe 650-0047, Japan

microRNA-9-2 **and** ***microRNA-9-3*** **double-mutant mice demonstrate that** ***microRNA-9*** **(*miR-9*) controls neural progenitor proliferation and differentiation in the developing telencephalon by regulating the expression of multiple transcription factors. As suggested by our previous study, the Foxg1 expression was elevated, and the production of Cajal-Retzius cells and early-born neurons was suppressed in the *miR-9-2/3* double-mutant pallium. At embryonic day 16.5 (E16.5), however, the Foxg1 expression was no longer elevated. The expression of an AU-rich RNA-binding protein Elavl2 increased at E16.5, Elav2 associated with *Foxg1* 3′ untranslated region (UTR), and it countered the *Foxg1* suppression by miR-9. Later, progenitor proliferation was reduced in the *miR-9-2/3* double-mutant pallium with the decrease in Nr2e1 and Pax6 expression and the increase in Meis2 expression. The analyses suggest that *microRNA-9* indirectly inhibits *Pax6* expression by suppressing Meis2 expression. In contrast, together with Elavl1 and Msi1, *microRNA-9* targets *Nr2e1* mRNA 3′ UTR to enhance the expression. Concomitantly, cortical layers were reduced, each cortical projection was malformed, and the tangential migration of interneurons into the pallium was impaired in the *miR-9-2/3* double mutants. miR-9 also targets *Gsh2* 3′ UTR, and Gsh2, as well as Foxg1, expression was elevated in the *miR-9-2/3* double-mutant subpallium. The subpallium progenitor proliferation was enhanced, and the development of basal ganglia including striatum and globus pallidus was suppressed. Pallial/subpallial boundary shifted dorsally, and the ventral pallium was lost. Corridor was malformed, and thalamocortical and corticofugal axons were misrouted in the *miR-9-2/3* double mutants.**

Introduction

Development of mammalian telencephalon depends on the highly ordered regulation of neural progenitor proliferation/differentiation and neuronal migration. In the pallium, younger projection neurons migrate radially and settle between the marginal zone and subplate to create the cortical plate in an inside-out manner. Cajal-Retzius cells in the marginal zone provide a critical instructive cue in the six-layer formation (Huang, 2009). The cortical projection neurons are generated from two major progenitor pools: radial glia in the ventricular zone (VZ) and intermediate progenitor cells (IPCs) in the subventricular zone (SVZ) (Guillemot et al., 2006). Several transcription factors control the proliferation/differentiation of these cells. Foxg1 regulates progenitor proliferation and Cajal-Retzius cell differentiation (Dou et al., 1999; Hanashima et al., 2002, 2004; Martynoga et al., 2005; Muzio and Mallamaci, 2005). *Ngn1/2* and *Tbr1* regulate the production of early-born neurons, *Tbr2* directs IPC generation, and *Pax6*, *Nr2e1/Tlx*, and *Id4* regulate the generation of later-born neurons (Yun et al., 2004; Bedford et al., 2005; Guillemot et al., 2006; Molyneaux et al., 2007). In the subpallium, lateral (LGE) and medial (MGE) ganglionic eminences generate distinct nuclei, including the striatum and the globus pallidus, respectively. The proliferation/differentiation of the subpallial progenitor cells are regulated by Mash1, Dlx1/2/5/6, Nkx2.1, and Gsh2 (Anderson et al., 1997; Horton et al., 1999; Sussel et al., 1999; Toresson et al., 2000; Yun et al., 2001; Flames et al., 2007; Molero et al., 2009).

The expression of these genes must be finely regulated for proper neurogenesis. microRNAs are small, noncoding RNAs that typically bind to specific sequences in the 3′ untranslated regions (3′ UTR) of target mRNAs to fine-tune protein expression (Bartel, 2009). Conditional mutants of the *Dicer1* gene, which is essential to the biosynthesis of almost all microRNAs, have indicated that microRNAs are required for brain development (De Pietri Tonelli et al., 2008). However, the contribution of each microRNA has been essentially unexplored. *microRNA-9* (*miR-9*) and complementary *miR-9** are abundantly expressed in vertebrate brains (Lagos-Quintana et al., 2002; Griffiths-Jones, 2006; Kloosterman et al., 2006). In zebrafish, a knockdown study demonstrated that *miR-9* modulates the organizing activity of the midbrain–hindbrain boundary by suppressing Fgf signaling pathway (Leucht et al., 2008). Several studies have suggested that *miR-9/miR-9** targets *Nr2e1*, *REST*, *CoREST*, and *BAF53a* to suppress progenitor proliferation and promotes neural differentia-

Received Sept. 28, 2010; revised Nov. 28, 2010; accepted Dec. 20, 2010.

This work was supported by a Grant-in-Aid for Creative Scientific Research from the Japan Society for the Promotion of Science. We are indebted to the Laboratory for Animal Resources and Genetic Engineering, RIKEN Center for Developmental Biology (CDB), for their help in the generation and housing of the mutant mice. We acknowledge Dr. Y. Sasai of RIKEN CDB for the Foxg1 antibody, Dr. K. Campbell of the University of Cincinnati College of Medicine for the Gsh2 antibody, and Dr. Y. Hayashizaki of RIKEN Omics Science Center and the Genome Resource and Analysis unit of RIKEN CDB for providing us FANTOM3 clones. We also thank those who provided us with probes for RNA *in situ* hybridization.

Correspondence should be addressed to Shinichi Aizawa, Laboratories for Vertebrate Body Plan and for Animal Resources and Genetic Engineering, Center for Developmental Biology, RIKEN Kobe, 2-2-3 Minatojima-minamimachi, Chuo-ku, Kobe 650-0047, Japan. E-mail: saizawa@cdb.riken.jp.

DOI:10.1523/JNEUROSCI.5085-10.2011

 0270-6474/11/313407-16$15.00/0

tion (Packer et al., 2008; Yoo et al., 2009; Zhao et al., 2009). *miR-9* promotes proliferation of human embryonic stem cell-derived neural progenitors by targeting *stathmin* (Delaloy et al., 2010). We have proposed that *miR-9* targets *Foxg1* to regulate Cajal-Retzius cell production (Shibata et al., 2008). In this study, we generated mutant mice lacking *miR-9-2* and *miR-9-3* (referred to as *miR-9-2/3* double mutants) to examine the *miR-9/miR-9** functions in telencephalic development. *miR-9-2/3* double mutants exhibited dysregulation of pallial and subpallial progenitor proliferation/differentiation. Concomitantly, the double mutants exhibited multiple defects in the telencephalic structures. These defects are considered to be brought about by the dysregulation of Foxg1, Nr2e1, Gsh2, and Meis2 expression. Furthermore, we propose that *miR-9* functions are modulated by RNA-binding proteins.

Materials and Methods

Generation of miR-9-2 and miR-9-3 mutant mice. microRNA-9-2 and *microRNA-9-3* mutant mice (Center for Developmental Biology accession numbers CDB0072K and CDB0071K; http://www.cdb.riken.jp/arg/mutant%20mice%20list.html) were generated by gene targeting with TT2 embryonic stem cells as described previously (Yagi et al., 1993). Genomic DNA fragments were isolated by long-amplification PCR with C57BL/6 BAC clones to construct the targeting vector (Murata et al., 2004). The PrDT-A pA cassette is the diphtheria toxin A fragment gene with an MC1 promoter and β-globin poly(A) signal, and the PrNeo poly(A) cassette is the neomycin-resistant gene with a *Pgk1* promoter and simian virus 40 (*SV40*) poly(A) signal; they were flanked by *loxP* sequences as described (http://www.cdb.riken.jp/arg/cassette.html). Chimeras were mated, and mutant mice were maintained by mating with C57BL/6 mice. Southern hybridization to identify the mutants was performed as described (Murata et al., 2004). Details of the targeting strategy will be provided on request. Genotyping of mice or embryos was routinely performed with specimens of tail, yolk sac, or a part of embryonic tissue by PCR using a mixture of two or three primers. Primer sets used are p1 (AAACTCCTTCAAGGTCACCGAG), p2 (CCCTTTTCCCTGCTAGCTCTAAG), p3 (ACCCGTGATATTGCTGAAGAGCTTGG), p4 (CCTTTGCCTTCACCCCATAA), and p5 (CGTCCGACCAGAACTATAGAGGTTTA), of which locations are indicated in supplemental Figure 2 (available at www.jneurosci.org as supplemental material). The PCR with p1–p3 primers yields 517 and 624 bp products for the wild-type (WT) and mutant (MT) *miR-9-2* alleles and with p3–p5 606 and 856 bp products for the wild-type and mutant *miR-9-3* alleles, respectively. Two mutant mouse lines were established from independent homologous recombinant embryonic stem cell clones of both *miR-9-2* and *miR-9-3* loci; no difference in phenotype was observed between the two mutant lines of each locus. Two independent lines were also established for *miR-9-2/3* double mutants, giving no apparent difference in phenotype. *miR-9-2* single homozygous pups died within 1 month of birth; *miR-9-3* single homozygous pups grew to adulthood, but both male and female homozygous mutants were infertile. *miR-9-3* homozygous and *miR-9-2* heterozygous double mutants died within 1 month of birth, and *miR-9-2/3* double homozygous mutants were obtained by crosses between double heterozygotes. Mice were housed in environmentally controlled rooms of the Animal Housing Facility of the Center for Developmental Biology, RIKEN Kobe under the institute guidelines for animal and recombinant DNA experiments.

Plasmid construction. The procedure to generate *luciferase* reporter and expression vector was described previously (Shibata et al., 2008). To generate luciferase reporter constructs, wild-type and mutant DNA fragments harboring the putative *miR-9* responsive elements from the *Meis2*, *Islet1*, *Gsh2*, and *Pax6* 3′ UTRs were synthesized as DNA oligonucleotides. Their sizes were 48–52 bp, and target sequences were placed in the middle of each fragment: top strand, 5′-ggCGTCTCTGGGCTGATTACTTAACCAAAGACAAAATAATGAGTCCTAA-3′ and bottom strand, 5′-ccTTAGGACTCATTATTTTGTCTTTGGTTAAGTAATCAGCCCAGAGACG-3′ for *Meis2*; top strand, 5′-ggCGTCTCTGGGCTGATTACTTAAC**GTTT**GACAAAATAATGAGTCCTAA-3′ and bottom strand, 5′-ccTTAGGACTCATTATTTTGTC**AAAC**GTTAAGTAATCAGCCCAGAGACG-3′ for mutant *Meis2*; top strand, 5′-ccTGTCTGTCCAAGAACTTTTCCCCCAAAGATGTGTATAGTTATTGGTTA-3′ and bottom strand, 5′-ggTAACCAATAACTATACACATCTTTGGGGGAAAAGTTCTTGGACAGACA-3′ for *Islet1*; top strand, 5′-ccTGTCTGTCCAAGAACTTTTCCCC**GTTT**GATGTGTATAGTTATTGGTTA-3′ and bottom strand, 5′-ggTAACCAATAACTATACACAT**CAAAC**GGGGAAAAGTTCTTGGACAGACA-3′ for mutant *Islet1*; top strand, 5′-ggCTCCTCCCCATCAGCACAGGGACCAAAGTTCTAGTCCATTGCCCTCAT-3′ and bottom strand, 5′-ccATGAGGGCAATGGACTAGAACTTTGGTCCCTGTGCTGATGGGGAGGAG-3′ for *Gsh2*; top strand, 5′-ggCTCCTCCCCATCAGCACAGGGAC**GTTT**GTTCTAGTCCATTGCCCTCAT-3′ and bottom strand, 5′-ccATGAGGGCAATGGACTAGAAC**AAAC**GTCCCTGTGCTGATGGGGAGGAG-3′ for mutant *Gsh2*; and top strand, 5′-ggGGAGCCCGGGAATGGACTAGAACCAAGGACCTTTGCGTACAGAAGGC-3′ and bottom strand, 5′-ccGCCTTCTGTACGCAAAGGTCCTTGGTTCTAGTCCATT CCCGGGCTCC-3′ for *Pax6*. Underlining indicate sequences predicted to base pair with the seed sequence of *miR-9*; bold letters indicate mutated nucleotides. To construct reporters with mutant *Foxg1* 3′ UTR in Figure 4*D* (*Foxg1* 3′ UTR *MT1*, *MT2*, *MT1* + *2*, and *MT3*), T and A were substituted by G and C, respectively, as indicated. For the *Nr2e1* reporter construct, a DNA fragment containing the full-length *Nr2e1* 3′ UTR (1398 bp) was amplified from clone 3425403H08, obtained from the Functional Annotation of Mouse-3 (FANTOM3) library (Carninci et al., 2005). *Foxg1* reporter (*luc–Foxg1*), pEF1α–*miR-9-2Wt* and pEF1α–*miR-9-2Mt* were constructed previously (Shibata et al., 2008).

To express *Elavl1*, *Elavl2*, *Elavl4*, and *Msi1* in the P19 cells, the protein-coding regions of *Elavl1* (clone A630073F18; FANTOM3), *Elavl2* (IMAGE identification number 6821133; Open Biosystems), *Elavl4* (clone 3110037G03; FANTOM3), and *Musashi1* (clone D130076N11; FANTOM3) cDNAs were amplified by PCR and inserted into the pEF-1α vector (Invitrogen). Primer sets used were as follows: forward, 5′-ataagaatgcggccgcATGTCTAATGGTTATGA-3′ and reverse, 5′-atagtttagcggccgcTTATTTGTGGGACTTGT-3′ for *Elavl1*; forward, 5′-ataagaatgcggccgcAACAAAGCAATATGAGGT-3′ and reverse, 5′-atagtttagcggccgcTTAGGCTTTGTGCGTTT-3′ for *Elavl2*; forward, 5′-ataagaatgcggccgcATGGAGTGGAATGGCTT-3′ and reverse, 5′-atagtttagcggccgcTCAGGATTTGTGGGCTT-3′ for *Elavl4*; and forward, 5′-ataagaatgcggccgccaccATGTTCATCGGAGGACTCAG-3′ and reverse, 5′-atagtttagcggccgcTTACCTCCGTCTGCCTG-3′ for *Msi1*. Lowercase letters indicate linker sequences, and underlining indicate the NotI site. To express wild-type or mutant *miR-9-2* in the P19 cells, ~200 bp of wild-type or mutant DNA fragments obtained in the previous study (Shibata et al., 2008) were inserted into a modified pGK vector (Gene Bridge) at the NotI site to produce pGK–*miR-9-2Wt* or pGK–*miR-9-2Mt*. For electroporation into the telencephalon, the protein-coding region of a human *Gsh2* cDNA clone (IMAGE identification number 30915389; Open Biosystems) and mouse *Foxg1* cDNA (IMAGE identification number 6314329; Open Biosystems) were amplified by PCR and inserted into pCMS–EGFP vector (*SV40–EGFP*; Clontech). Primer sets used were as follows: forward, 5′-gctctagacaccATGTCGCGCTCCTTCTA-3′ (underlining indicates XbaI site) and reverse, 5′-gctctagaTCATAAGGGGGAAATCT-3′ for *Gsh2*; and forward, 5′-ggaattccaccATGCTGGACATGGGAGATAG-3′ (underlining indicates EcoRI site) and reverse, 5′-gctctagaCTAATGTATTAAAGGGTTGG-3′ (underlining indicates XbaI site) for *Foxg1*. Lowercase letters indicate linker sequences.

In situ *hybridization.* Section *in situ* hybridization using antisense DIG-labeled RNA was performed as described previously (Shibata et al., 2008). All cDNAs used for the DIG–RNA probe synthesis were obtained from the FANTOM3 library, except for *Wnt3a* and *Svet1*. cDNAs for *Wnt3a* and *Svet1* probes were gifts from Drs. A. McMahon (Harvard University, Cambridge, MA) and P. Gruss (Max Planck Institute of Biophysical Chemistry, Göttingen, Germany), respectively. To detect *miR-9-1* and *miR-9-3* precursors, 244 and 397 bp DNA fragments containing loop and *miR-9** sequences were amplified from the mouse genome using T7-tagged reverse primers, and amplified PCR fragments were used as templates to generate probes. Primer sets used were as follows: forward, 5′-AGTGGTGTGGAGTCTTCATAAAGCT-3′ and reverse,

5′-ccggatcctaatacgactcactatagggCCAGAGCGGCTTCTTGCTT-3′ (lowercase letters indicate T7 promoter) for *miR-9-1*; and forward, 5′-AGTGCCACAGAGCCGTCATAA-3′ and reverse, 5′-ccggatcctaatacgactcactatagggGCGTGGATTGTTCTAGCCTGAT-3′ for *miR-9-3*. For the detection of *miR-9-2*, a cDNA clone (IMAGE identification number 6819393; Open Biosystems) was used as a template to generate probes. The *in situ* hybridization data were confirmed by repeating the assay more than twice with independent embryos from different litters.

Quantitative reverse transcription-PCR for RNAs. cDNAs were prepared from more than three independent wild-type and *miR-9-2/3* double-mutant cerebral hemispheres from different litters, and quantitative reverse transcription (RT)-PCR was performed as described previously (Shibata et al., 2008). At least three replicates per transcript were used for every reaction. Assays were repeated at least three times. Data are expressed as means ± SD. The copy number of transcripts was normalized against the TATA-binding protein transcript level, and the ratio is shown as relative transcript level in Figures 1*A*, 2*C*, 6*D*, 7*B*,*F*, and 8*B*,*D* and supplemental Figures 1*B* and 2*G* (available at www.jneurosci.org as supplemental material). For all tested primer sets, correlation (R^2) was higher than 0.98, and the slope was −3.1 to −3.6 in each standard curve. Primers to detect *Foxg1*, the *TATA binding protein*, *miR-9-1*, *miR-9-2*, and *miR-9-3* RNAs were described previously (Shibata et al., 2008). Primers to detect the expression of the following genes were designed in a single exon encoding the 3′ UTR: forward, 5′-CTAACCATGGCCAAGAGCTCA-3′ and reverse, 5′-CTGACCAAAGCATGTGGCTG-3′ for *Foxp2*; forward, 5′-ACAGGCTGAGCCAGGTTCTG-3′ and reverse, 5′-AATGATTCAGCGGGATCTTCC-3′ for *Nr2e1*; forward, 5′-GAAATGGCGGTTAGAAGCACTT-3′ and reverse, 5′-GGGCTCCAGTTCAGGACAGTT-3′ for *Pax6*; forward, 5′-CCAGGCCCTCCAGAGACAC-3′ and reverse, 5′-TCATTGGTGCCTGGGCTTAC-3′ for *Elavl1*; forward, 5′-CTGCCTCTCTCCCTGGTCG-3′ and reverse, 5′-GGGCAACTGGCTAATCCAAAA-3′ for *Msi1*; forward, 5′- GGGAGTGACAGCGAAAACCA-3′ and reverse, 5′-TGGCCCTTATCAGTTGGCTT-3′ for *Sox5*; and forward, 5′-GCTCTTTCACTTGACCCTCGA-3′ and reverse, 5′-GAGACCTGCACTTATCCCCG-3′ for *Tbr1*. Primers to detect the expression of transcripts surrounding each *miR-9* precursor as shown in supplemental Figure 1*B* (available at www.jneurosci.org as supplemental material): forward, 5′-ACCCGGCAAGTGGTGACTAC-3′ and reverse, 5′-TTAGGTGACAGGCGTGTTCCT-3′ for *Mef2C*; forward, 5′-GGCTGGTTCTCTGTCCTGCT-3′ and reverse, 5′-CCCTTCTAGGGCACTGCATC-3′ for *Polγ*; forward, 5′-CCCATTAGCTGTGGCCAGAA-3′ and reverse, 5′-GGTGGCAGTCACCTAGGCTG-3′ for *Rhcg*; forward, 5′-ATTCCCCTGCGTACCTTGC-3′ and reverse, 5′-CAGCTTCCGCACGACTTTTT-3′ for *hs_Smarce1*; forward, 5′-GCATAGGCAGGCAGATGGAA-3′ and reverse, 5′-GAGGCCCTGCTTTAAGCAATAG-3′ for the RT-PCR product "a" in *AK043150*; forward, 5′-GTTGGCTAACGATACTGGAGATTACTT-3′ and reverse, 5′-TTATTCCAAACTTTTCCCCTTCC-3′ for "b" in *BC096523*; forward, 5′-TTACTCTGCGCCTAGCATTGG-3′ and reverse, 5′-TTTTTTGTGGCGTAAATGTCACTT-3′ for "c" in *BC096523*; forward, 5′-CGCTGTACACGTGCCAAAGTT-3′ and reverse, 5′-GGGTCTTCTCGACTGCCTCTAC-3′ for "d" in *AK048540*; forward, 5′-AGCCTGGAGACTCGCCTGAT-3′ and reverse, 5′-GGTTGTGGTGATGGTGGTT-3′ for "e" in *AK032343*; forward, 5′-AACCACCATCACCACAACC-3′ and reverse, 5′-TCTTTTCTCCTGGCCCAC-3′ for "f" in *AK032343*; forward, 5′-TGATGACTAAGAAGATTGTCCTGTGAA-3′ and reverse, 5′-TCAGAGCCTGTGCCATCACTT-3′ for "g" in *AK032343*; and forward, 5′-TGTTCTGTGCCTGAGAACGG-3′ and reverse, 5′-CGAGTGTGCCCTTGAACCTC-3′ for "h" in *AK032343*.

miR-9 and miR-9 quantification.* Total RNAs were isolated from wild-type and *miR-9-2/3* double-mutant telencephalon using a mirVana miRNA Isolation kit (Ambion). Quantitative RT-PCR was performed using a Taqman microRNA Reverse Transcription kit (Ambion) and Taqman Universal Master MixII, noUNG (Ambion) according to the instructions of the manufacturer. The *snoRNA202* was used as an endogenous internal control for normalization; after the normalization, each transcript level was shown as the relative ratio to the level in E16.5 wild-type cerebral hemispheres (supplemental Fig. 2*H*,*I*, available at www.jneurosci.org as supplemental material). Assays were repeated at least three times with two independent embryos from different litters. Data are presented as means ± SD.

Immunoblot, immunohistochemistry, and histology. Immunoblot and immunohistochemistry were performed as described (Shibata et al., 2008). Each immunoblotting was repeated more than two times with independent embryos from different litters, and representative results are presented in Figures 2*B*, 7*A*,*E*, 9*R*, and 10*L*. Quantification of band intensity was performed with NIH ImageJ software (Abramoff et al., 2004). Immunohistology was also confirmed by repeating the assay more than twice with independent embryos from different litters. For immunohistochemistry, the brain was dissected from each embryo and fixed with 4% paraformaldehyde overnight at 4°C, followed by embedding in OCT and sectioning at 14 μm. For antigen retrieval, sections were treated with HistoVT One (Nacalai Tesque) for 20 min at 72°C. For the detection of bromodeoxyuridine (BrdU) distribution in the pallium, sections were treated in 1N HCl for 10 min at room temperature and then in 2N HCl for 40 min at 37°C to denature DNA, followed by a rinse with PBS and the antigen retrieval. Nissl staining was performed using standard procedure. terminal deoxynucleotidyl transferase-mediated biotinylated UTP nick end labeling (TUNEL) assay was performed with the In Situ Cell Death Detection kit (Roche) according to the instructions of the manufacturer. The sources of antibodies used are as follows: primary antibodies used for immunohistochemistry were anti-Foxg1 (1:500) (Watanabe et al., 2005), anti-active caspase3 (1:500; Promega), anti-Gsh2 (1:5000) (Toresson et al., 2000), anti-Tuj1 (1:500; Covance), anti-calretinin (1:1000; Millipore Bioscience Research Reagents), anti-Id4 (1:500; Santa Cruz Biotechnology), anti-Nestin (1:100; BD Pharmingen), anti-BrdU (1:100; BD Pharmingen), anti-Ctip2 (1:500; Abcam), anti-Sox5 (1:200; Abcam), anti-Ki67 (1:200; Thermo Fisher Scientific), anti-L1 (1:200; Millipore Bioscience Research Reagents), anti-TAG1 (whole serum; Developmental Studies Hybridoma Bank), anti-GAP43 (1:2000; Zymed), anti-chondroitin sulfate proteoglycans (CSPGs) (1:200; Sigma), anti-Meis2 (1:500; Santa Cruz Biotechnology), and anti-Pax6 (1:500; Covance). Secondary antibodies were conjugated with Alexa Fluor 488 or 594 (1:200; Invitrogen). The anti-TAG1 antibody (4D7) developed by M. Yamamoto was obtained from the Developmental Studies Hybridoma Bank under the auspices of the National Institute of Child Health and Human Development and maintained by the University of Iowa, Department of Biology (Iowa City, IA). Primary antibodies used for immunoblot were anti-Nr2E1 (1:500; Perseus Proteomics), anti-Ngn2 (1:200; US Biological), anti-Foxg1 (1:1000) (Watanabe et al., 2005), anti-Gsh2 (1:5000) (Toresson et al., 2000), anti-Islet1 (1:200; Abcam), anti-Elavl2 (1:500; Abcam), and anti-glyceraldehyde-3-phosphate dehydrogenase (Gapdh) (1:5000; Abcam). Secondary antibodies were conjugated to horseradish peroxidase (1: 2000; Millipore or Cell Signaling Technology).

Image processing. Several photographs of a section taken at the same time were assembled into single images shown in Figures 1*E*,*F*, 2*A*, 5*A*,*E*, 6*A*,*B*, and 9*A–D*″,*M–N*′,*S*,*U*.

RNA affinity precipitation assay. The RNA affinity precipitation assay was performed as described previously (Wakiyama et al., 2007) with minor modifications. Mouse cortices at E17.5 were homogenized in radioimmunoprecipitation assay buffer, and homogenate was adjusted to 5 mg/ml. Ten microliters of lysates were diluted in 500 μl of binding buffer [20 mM HEPES-KOH at pH 7.4, 150 mM NaCl, 1.5 mM $MgCl_2$, 5% glycerol, 0.1% Triton X-100, 1.5 mM dithiothreitol, 0.2 mg/ml heparin, 0.2 mg/ml tRNA (Ambion), 0.25% BSA (Ambion), protease inhibitor cocktail (Roche Diagnostics), and ribonuclease inhibitor (Invitrogen)]. The mixtures were incubated with or without biotinylated RNA (2 μg) for 10 min at 16°C. Adding Dynabeads Myone Streptavidin T1 (Invitrogen), preequilibrated in the binding buffer, the mixtures were further incubated for 15 min at 4°C. The beads were then captured with a magnet, washed four times with 500 μl of the wash buffer (20 mM HEPES-KOH at pH 7.4, 150 mM NaCl, 1.5 mM $MgCl_2$, 5% glycerol, 0.1% Triton X-100, 1.5 mM dithiothreitol, and 0.2 mg/ml heparin), and boiled with 20 μl of SDS sample buffer. The supernatant was resolved on 10% polyacrylamide gels and subjected to the Elavl2 immunoblot. Biotinylated Foxg1 3′ UTR (both wild-type *Foxg1 3′ UTR WT* and mutated *Foxg1 3′ UTR MT1*) fragments were purchased from Gene Design.

Cell culture and transfection. Cell culture and transfection for luciferase assays were performed with P19 cells as described (Shibata et al., 2008); P19 cells were treated with 500 nM retinoic acid for 2 d after transfection.

Dissociation of and electroporation into cortical cells in culture were conducted as described previously (Shibata et al., 2008).

Luciferase assay. Luciferase assay was performed with P19 cells using a Dual-Glo Luciferase Assay system (Promega) as described previously (Shibata et al., 2008); Renilla reniformis luciferase expression vector was cotransfected for normalization. For each sample, four replicates were measured in a single assay. Assays were repeated at least three times, and representative results are shown. Data are expressed as means ± SD of four replicates. In Figure 4, *B* and *D*, *miR-9-2* precursor RNA and its control oligo RNA were purchased from Ambion and transfected into P19 cells. In Figures 6*C*, 7*C*,*D*, 9*Q*, and 10*K*, *miR-9* was expressed by transfecting *miR-9-2* precursor in *pEF1α* or *pGK* expression vector, and the vector served as control. The relative luciferase activity is given as the relative ratio to the activity observed by the control (oligo RNA, *pEF1α*, or *pGK*) transfection.

BrdU labeling. For the pulse labeling of cells in S phase, timed pregnant female mice at E12.5, E13.5, and E15.5 were injected intraperitoneally with a single pulse of BrdU (Roche) (50 mg/kg body weight) and killed after 30 min or after 24 h for the dissection of embryonic brains. For birthdating analyses, BrdU was injected at E14.5, and the distribution of BrdU-positive cells in the embryonic pallium was determined at E18.5 as described previously (Schuurmans et al., 2004).

Quantification of BrdU-positive, Ki67-positive, and pH3-positive cells. In Figure 3, *V* and *W*, three anatomically matched cortical sections 84 μm apart were selected from wild-type and *miR-9-2/3* double-mutant cortices. They were immunostained with the anti-BrdU antibody, two anatomically matched 270 × 200 μm areas, including the entire ventricular–pial axis, were selected, and the BrdU-positive cells in the areas were counted. For E13.5 cortex, areas were divided into the VZ and SVZ according to *Tbr2* expression, and the BrdU-positive cells in VZ and SVZ were counted. In Figure 3*X*, three anatomically matched cortical sections 84 μm apart from three cortices of both genotypes were stained with the anti-phospho-histone H3 antibody, and two anatomically matched 200 × 200 μm areas were selected and divided into the VZ and SVZ according to *Tbr2* expression for counting. In Figure 5*B–D*, three anatomically matched cortical sections 168 μm apart from wild-type and *miR-9-2/3* double-mutant cortices were immunostained with anti-BrdU and anti-Ki67 antibodies, and five anatomically matched 200 × 100 μm areas in the VZ and 200 × 200 μm (wild-type) or 200 × 150 μm (*miR-9-2/3* double mutant) areas in the SVZ were selected for counting. In Figure 5*F*, two anatomically matched 400 × 100 μm areas of both genotypes were selected for the counting. The VZ and SVZ in Figure 5*B–F* were defined by *Tbr2* or *Svet1* expression, respectively, detected by *in situ* hybridization of adjacent sections. In Figure 9*M–P* and supplemental Figure 7*A–F* (available at www.jneurosci.org as supplemental material), BrdU- and Ki67-positive cells were counted in four and three, respectively, 180 × 100 μm bins along the ventricular–pial axis of the LGE. Three anatomically matched cortical sections 168 μm (see Fig. 9*M–P*) or 84 μm (supplemental Fig. 7*A–F*, available at www.jneurosci.org as supplemental material) apart were chosen for the counting. All these assays were repeated more than twice with three independent embryos from different litters. Data are presented as means ± SD. Unpaired two-tailed Student's *t* tests were performed, and *p* values are given in each figure.

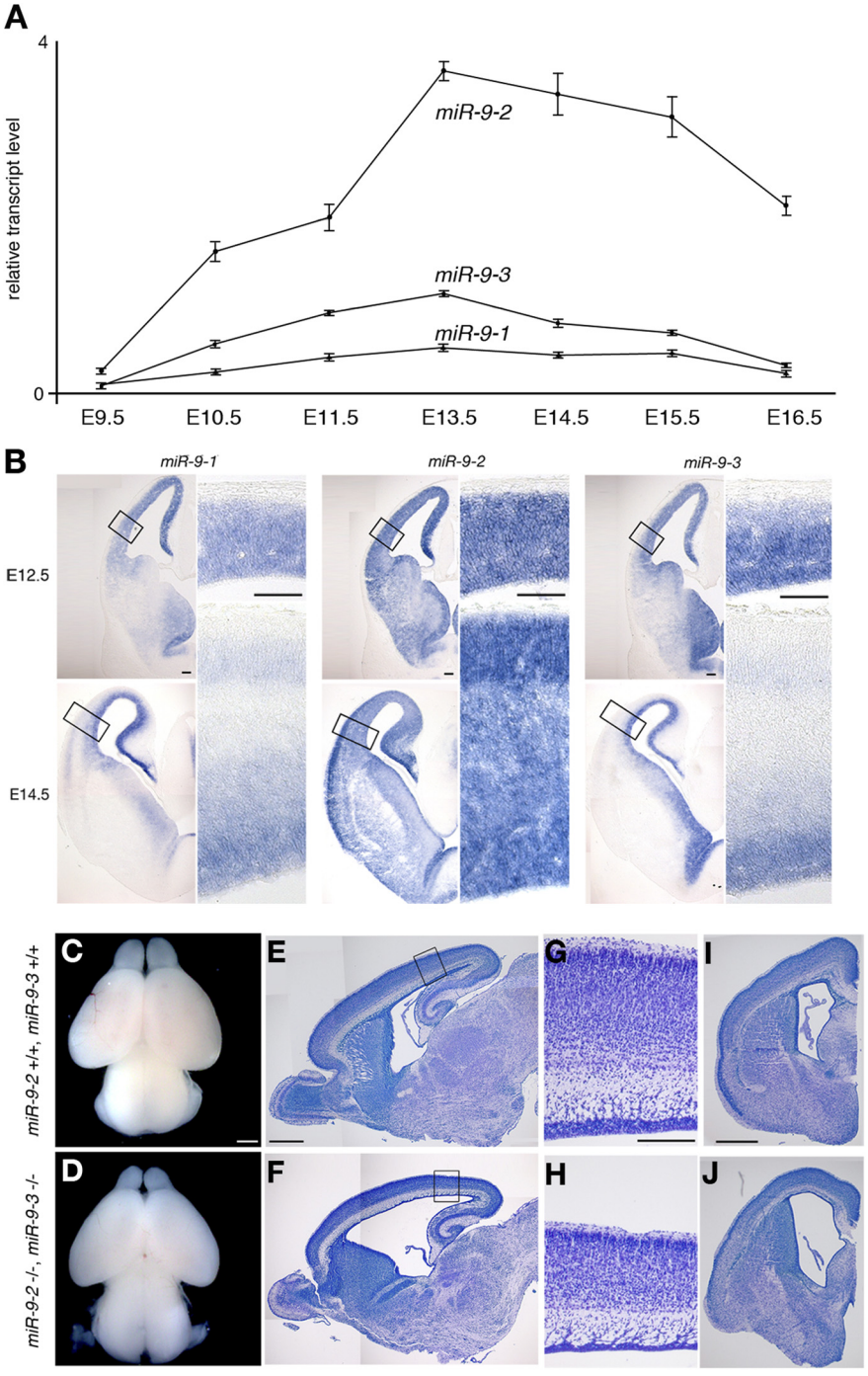

Figure 1. *miR-9-2/3* double mutation. ***A***, Quantitative RT-PCR analyses of expression levels of *miR-9* precursors in developing cerebral hemispheres at the indicated stages. See Materials and Methods for relative transcript level. ***B***, Expression pattern of each *miR-9* precursor in E12.5 and E14.5 telencephalon by RNA *in situ* hybridization. In each *miR-9* precursor expression, the right panels give enlarged views of the areas boxed in the left panels. ***C–J***, Gross phenotypes of *miR-9-2/3* double mutants at P1. Dorsal views (***C***, ***D***), parasagittal sections (***E***, ***F***), and frontal sections at the telencephalic level (***I***, ***J***) of F2 wild-type and *miR-9-2/3* double-mutant brains, respectively. ***G*** and ***H*** gives enlarged views of the cortices boxed in ***E*** and ***F***. ***E–J***, Nissl staining. Scale bars: ***B***, 100 μm; ***C–F***, ***I***, ***J***, 500 μm; ***G***, ***H***, 200 μm.

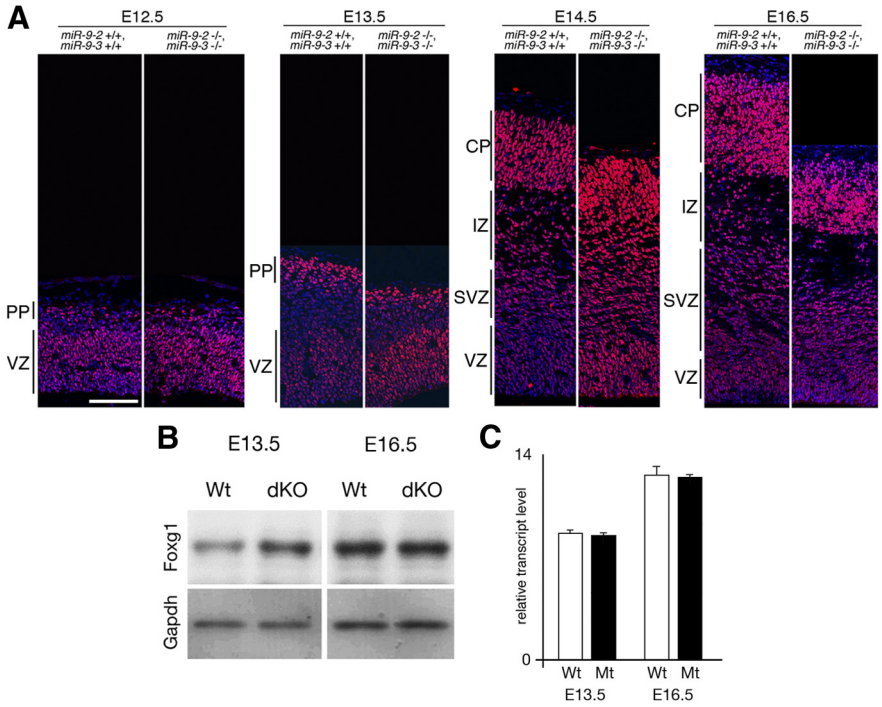

Figure 2. Foxg1 expression in *miR-9-2/3* double-mutant pallium. ***A***, Immunostaining with an anti-Foxg1 antibody of cortices at indicated stages. Layers are indicated as VZ, preplate (PP), SVZ, intermediate zone (IZ), and cortical plate (CP). ***B***, Western blotting for Foxg1 expression in cerebral hemispheres dissected at E13.5 and E16.5. Relative intensities of Foxg1 bands in the double mutant are 2.0-fold and 1.0-fold of the wild type at E13.5 and E16.5, respectively, as estimated by normalizing the intensities against those of Gapdh bands. ***C***, Quantitative RT-PCR for *Foxg1* transcripts. Wt, Wild type; Mt, *miR-9-2/-3* double mutant; dKO, double knockout. Scale bar, 100 μm.

Exo utero *electroporation*. *Exo utero* electroporation of DNA constructs into the cortex was performed as described previously (Shibata et al., 2008). *Gsh2* (see Fig. 9*T*) or *Foxg1* (see Fig. 9*V*) transgene under the cytomegalovirus promoter was conjugated to enhanced green fluorescent protein (*EGFP*) under the SV40 promoter and electroporated into the subpallium. In an assay, two anatomically matched sections 84 μm apart were selected from electroporated hemispheres. They were immunostained with the Ki67 and GFP antibody, anatomically matched 400 × 200 μm LGE areas were selected, and Ki67- and GFP-positive cells were counted. The assays were repeated more than two times with four independent embryos. Data are presented as means ± SD. Unpaired two-tailed Student's *t* tests were performed, and *p* values are given in the figures.

Results

Targeted deletion of miR-9-2 and miR-9-3

*miR-9/miR-9** has three precursors, *miR-9-1*, *miR-9-2*, and *miR-9-3* encoded in chromosomes 3, 13, and 7, respectively (Griffiths-Jones, 2006) (supplemental Fig. 1*A*, available at www.jneurosci.org as supplemental material). Quantitative RT-PCR revealed that *miR-9-2* is expressed most abundantly, *miR-9-3* much less so, and *miR-9-1* the least during telencephalon development (Shibata et al., 2008) (Fig. 1*A*). *In situ* hybridization demonstrated that, at E12.5 and E14.5, the *miR-9-2* is expressed throughout the telencephalon, whereas *miR-9-1* and *miR-9-3* are mostly localized in the proliferative zone (Fig. 1*B*). To assess the functions of *miR-9/miR-9** in telencephalon development, we mutated the *miR-9-2* and *miR-9-3* loci by replacing 72 and 90 nt, respectively, covering the mature *miR-9/miR-9** with a neomycin resistance cassette (supplemental Fig. 2, available at www.jneurosci.org as supplemental material). The double mutation abolished the *miR-9-2* and *miR-9-3* expression; no compensatory increase in *miR-9-1* expression was apparent (supplemental Fig. 2*G*, available at www.jneurosci.org as supplemental material). Consequently, mature *miR-9* expression was reduced to 24 and 23% of wild type in the *miR-9-2/3* double mutants at E12.5 and E16.5, respectively (supplemental Fig. 2*H*, available at www.jneurosci.org as supplemental material). The *miR-9** expression was decreased to 29 and 38% at E12.5 and E16.5, respectively (supplemental Fig. 2*I*, available at www.jneurosci.org as supplemental material).

The *miR-9-2/3* double mutants obtained by crosses between double heterozygotes were live born but exhibited severe growth retardation with small cerebral hemispheres and olfactory bulbs (Fig. 1*C*,*D*), and they died within 1 week. *miR-9-2/3* double mutants exhibited defects in other parts of the brain, especially in the inferior colliculus, but this study focused on the functions of *miR-9* in telencephalon development. Histological analyses at postnatal day 1 (P1) (Fig. 1*E–J*) showed marked reduction of the cortical layers and VZ; concomitantly, the lateral ventricles were expanded. In the subpallium, the proliferating zone was hyperplastic, whereas differentiated structures were reduced. Neither *miR-9-2* nor *miR-9-3* single homozygous mutants exhibited any apparent defects in neurogenesis of pallium or subpallium (supplemental Fig. 4, available at www.jneurosci.org as supplemental material) (data not shown), and the *miR-9-2/3* double-mutant defects are apparently attributable to *miR-9/miR-9** reduction (supplemental Figs. 1, 2, available at www.jneurosci.org as supplemental material).

miR-9 suppresses Foxg1 protein expression for the proper differentiation of Cajal-Retzius cells and early-born neurons

Foxg1 mRNA has *miR-9* responsive element in its 3′ UTR (supplemental Fig. 3, available at www.jneurosci.org as supplemental material); it does not have *miR-9** responsive element. The presence or absence of *miR-9* and *miR-9** responsive elements in a mRNA was assessed as described previously (Shibata et al., 2008) (also see Discussion). As suggested by our previous study (Shibata et al., 2008), the Foxg1 protein expression increased in the *miR-9-2/3* double-mutant VZ at E12.5–E14.5 (Fig. 2*A*,*B*; Table 1); *Foxg1* mRNA level was essentially unaffected (Fig. 2*C*). Concomitantly, cortical hem and the pallium/subpallium boundary (PSB)-derived Cajal-Retzius cells, marked by *p73* and *Ebf2*, respectively, were substantially reduced in the marginal zone at E12.5 and E13.5 (Fig. 3*A–D*) (data not shown). Consequently, *reelin*-positive Cajal-Retzius cells of multiple origins were greatly reduced in the marginal zone (Fig. 3*E*,*F*). The *Wnt3a*-positive domain and the differentiation of early neurons marked by Tuj1 or calretinin were also reduced in the cortical hem region (Fig. 3*G–J*) (supplemental Fig. 5*A*, available at www.jneurosci.org as supplemental material). *Dbx1*-positive ventral pallium from which *Ebf2*-positive Cajal-Retzius cells originate (Hanashima et al., 2007) was greatly reduced (Fig. 3*K*,*L*). The septum-derived Cajal-Retzius cells also appeared reduced in *miR-9-2/3* double mutants (supplemental Fig. 5*A*, available at www.jneurosci.org as supplemental material),

Table 1. *miR-9/miR-9 target candidates**

	Responsive element[a]		Reporter assay[b]			Expression in double mutants[c]	
Gene	*miR-9*	*miR-9**	I	II	Reference	Protein level	Reference
Foxg1	+	−	↓	DS (Elavl2)	Shibata et al., 2008; Fig. 4	↑ (E13.5)þNSC(E16.5)	Fig. 2
CoREST	+	+	↓ (*miR-9**)	NE	Packer et al., 2008	NSC (E13.5)	Data not shown
REST	+	+	↓ (*miR-9*)	NE	Packer et al., 2008	NSC (E13.5)	Data not shown
BAF53a	+	+	↓ (*miR-9**)	NE	Yoo et al., 2009	NSC (E13.5, 15.5)	Data not shown
Nr2e1	+	−	NSC	↑ (Elavl1, Msi1)	Fig. 7*C,D*	↓ (E13.5)	Fig. 7*A*
Nr2e1	+	−	↓	NE	Zhao et al., 2009	↓ (E13.5)	Fig. 7*A*
Id4	+	−	NSC	NE	Shibata et al., 2008	NSC (E12.5)	Fig. 3*M,N*
Pax6	+	−	NSC	NE	Fig. 6*C*	↓ (E15.5)	Fig. 6*A,B*
Meis2	+	−	↓	NE	Fig. 6*C*	↑ (E15.5)	Fig. 6*A,B*
Gsh2	+	−	↓	NE	Fig. 9*Q*	↑ (E15.5)	Fig. 9*R,S*
Islet1	+	−	m ↓	NE	Fig. 10*K*	m ↑ (E13.5)	Fig. 10*L*

[a] + indicates the presence and − the absence of the miR-9 or miR-9* responsive element in the mRNA of the gene indicated.

[b] Reporter assay with the cells given in the reference without (I) or with (II) the overexpression of an RNA-binding protein indicated in the parentheses. ↓ indicates the decrease and ↑ the increase in the expression by *miR-9* or *miR-9**. NSC, No significant change; DS, desupression; NE, not examined; m, moderate.

[c] Changes of the protein expression in *miR-9 –2/3* double mutants at the stage indicated in parentheses.

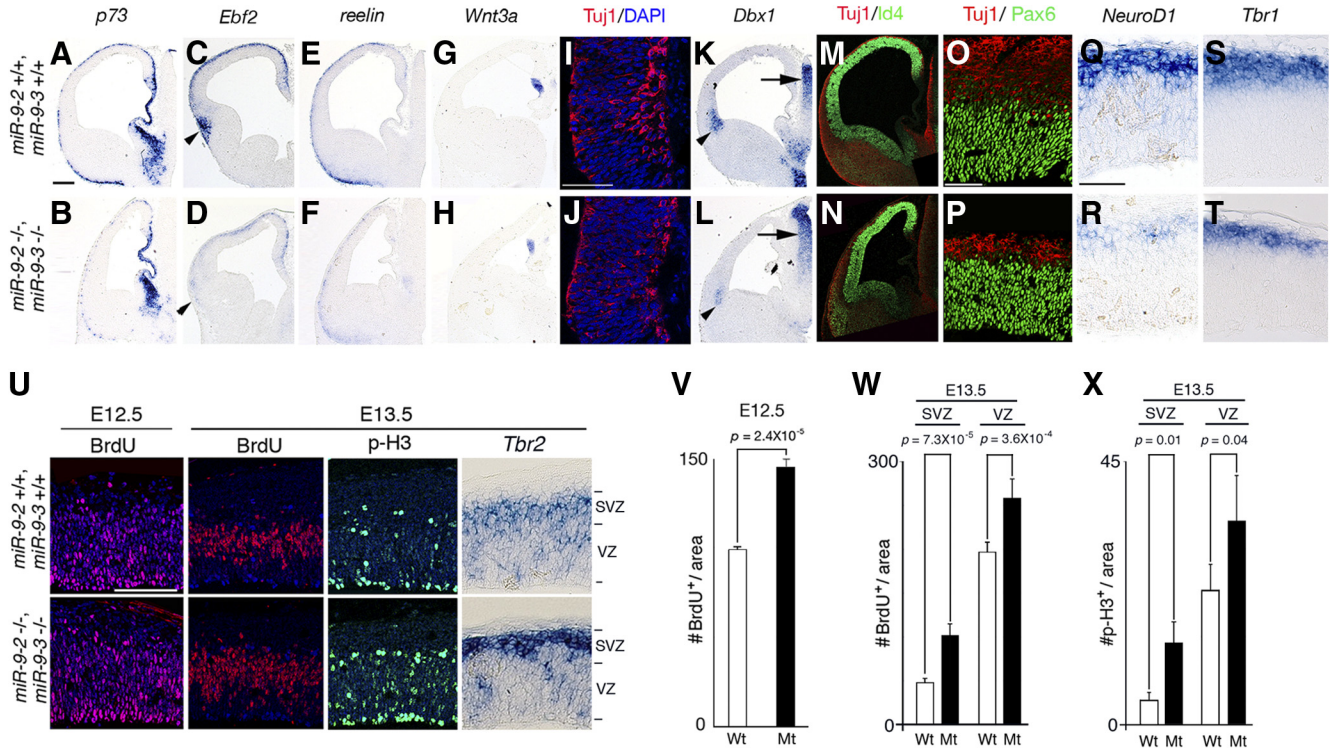

Figure 3. Early neurogenesis in *miR-9-2/3* double-mutant pallium. ***A–R***, Marker analyses of early-born neurons at E12.5. ***A–H***, ***K***, ***L***, and ***Q–T*** give RNA *in situ* hybridization for genes indicated; ***I***, ***J***, ***M–P***, immunostaining with an anti-Tuj1 antibody (red) and 4′,6′-diamidino-2-phenylindole (DAPI) (blue) at the cortical hem region (***I***, ***J***), with anti-Tuj1 antibody and an anti-Id4 antibody (green) in telencephalon (***M***, ***N***) or with anti-Tuj1 antibody and anti-Pax6 antibody (green) in the pallium (***O***, ***P***). Arrowheads in ***C***, ***D***, ***K***, and ***L*** indicate the ventral pallium, and arrows in ***K*** and ***L*** indicate the normal *Dbx1* expression in the thalamus. Scale bars: ***A–H***, ***K–N***, 200 μm; ***I***, ***J***, 100 μm; ***O–T***, 50 μm. ***U***, Typical examples of distribution of BrdU-incorporated cells after 30 min labeling, of distribution of phospho-histone H3-positive cells, and of RNA *in situ* hybridization for SVZ marker, *Tbr2* in the neopallium at either E12.5 or E13.5. ***V***, Quantification of BrdU-positive cells in the entire E12.5 pallium. ***W***, ***X***, Quantification of BrdU-positive cells (***W***) and phospho-histone H3-positive cells (***X***) in the VZ and SVZ at E13.5. Quantification in ***V–X*** was performed as described in Materials and Methods. Scale bar (in ***U***), 100 μm.

but more detailed analyses are required with specific markers. *Cxcl12*-positive meninges that are proposed to be the substrate for the tangential migration of Cajal-Retzius cells from the cortical hem (Huang, 2009) and *BMP7*- and *Msx1*-positive choroidal roof and choroid plexus developed normally (supplemental Fig. 5*A*, available at www.jneurosci.org as supplemental material). There were also no changes in the number of TUNEL-positive or active caspase3-positive cells (supplemental Fig. 5*A*, available at www.jneurosci.org as supplemental material).

Foxg1 has also been suggested to promote the proliferation of cortical progenitor cells in the VZ (Hanashima et al., 2002, 2004; Martynoga et al., 2005). In the E12.5 pallium, Id4- or Pax6-positive neuroepithelial cells were not significantly affected (Fig. 3*M–P*), and Nestin-positive radial glia cells were almost normal in the *miR-9-2/3* double mutants (supplemental Fig. 5*A*, available at www.jneurosci.org as supplemental material). However, early-differentiated Tuj1-, *NeuroD1*-, or *Tbr1*-positive neurons were significantly reduced in the preplate at E12.5 (Fig. 3*M–T*). Coincidentally, the calretinin-positive marginal zone and subplate and the CSPG- or GAP43-positive subplate were reduced in the *miR-9-2/3* double mutants at E18.5 (supplemental Fig. 5*B*,*C*, available at www.jneurosci.org as supplemental material) (Fig. 10*C–D*′).

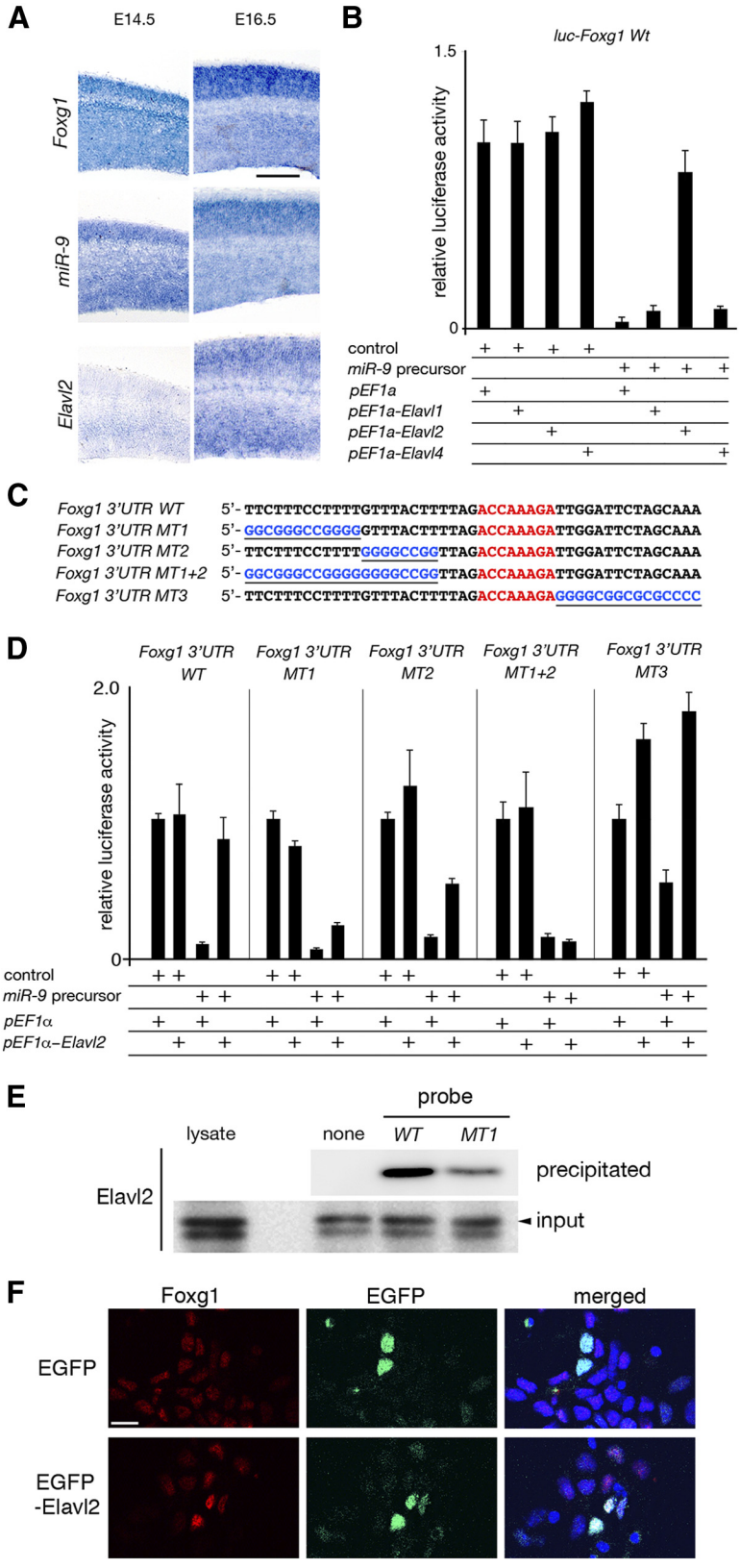

Figure 4. *Elavl2* counteraction of the *miR-9-2* suppression of Foxg1 expression. ***A***, RNA *in situ* hybridization of *Foxg1*, *miR-9*, and *Elavl2* expression in the wild-type neopallium at E14.5 and E16.5. ***B***, Effects of *Elavl* paralogs on the *miR-9-2* suppression of luciferase expression from a luciferase reporter conjugated to the *Foxg1 3′ UTR* in P19 cells. See Materials and Methods for relative luciferase activity. ***C***, Sequences of the wild-type *Foxg1* U-rich 3′ UTR and its mutant forms; *miR-9* responsive elements are indicated by red letters, and substituted sequences are underlined and in blue letters. ***D***, Luciferase expression from luciferase reporters conjugated to the wild-type and mutant *Foxg1 3′ UTRs* described in ***C***. ***E***, Elavl2 protein interaction with *Foxg1 3′ UTR*. Protein lysates from E17.5 cortices were incubated with biotinylated *Foxg1 3′ UTR WT* or *Foxg1 3′ UTR MT1* RNA probe. Probes were precipitated with streptavidin-coated beads, and bound Elavl2 protein was detected by Western blotting using anti-Elavl2 antibody. ***F***, Increase in Foxg1 expression by *Elavl2* overexpression in E12.5 cortical cells. E12.5 cortical cells were dissociated, electroporated with control *EGFP* or *EGFP--Elavl2* expression vector, and cultured for 48 h. Foxg1 expression was examined by immunostaining. Scale bars: ***A***, 200 μm; ***F***, 10 μm.

BrdU 30 min pulse labeling at E12.5 demonstrated that cell proliferation was increased by 56% in the *miR-9-2/3* double-mutant cortices compared with control cortices (Fig. 3*V*). At E13.5 BrdU incorporation was increased by 112 and 31% in the SVZ and VZ of the double-mutant cortices, respectively (Fig. 3*W*). Phospho-histone H3-positive mitotic cells were also increased by 230 and 47% in the SVZ and VZ, respectively (Fig. 3*X*). Concomitant with the increase in progenitor proliferation in the SVZ, *Tbr2* expression was enhanced in the SVZ (Fig. 3*U*). This is consistent with the report that IPCs are reduced by Foxg1 haploinsufficiency (Siegenthaler et al., 2008). Among genes suggested to regulate the production of early-born neurons (see Introduction), *Ngn1*, *Ngn2*, or *Tbr1* mRNAs do not have *miR-9/miR-9** responsive element. Among *miR-9/miR-9** targets demonstrated *in vitro* for progenitor proliferation (see Introduction), the protein expression of CoREST, REST, or BAF53a was not significantly changed in the E13.5 *miR-9-2/3* double-mutant telencephalon (Table 1).

Elavl2 attenuates the miR-9 suppression of Foxg1 expression

The increase in Foxg1 expression in *miR-9-2/3* double-mutant VZ was apparent at E14.5 but not from E16.5 onward (Fig. 2*A*,*B*). Even at these stages, *miR-9* and *Foxg1* expression overlapped (Fig. 4*A*), implying that *miR-9* suppression of *Foxg1* expression was attenuated as development proceeded. The *miR-430* suppression of Nanos1 and Tdrd7 protein expression has been reported to be cancelled by an AU-rich RNA binding protein Dnd1 in germ cells (Kedde et al., 2007). The 3′ UTR of *Foxg1* has U-rich sequences upstream of the *miR-9* responsive element (Fig. 4*C*). Elavl1/HuR, Elavl2/HuB, and Elavl4/HuD are the AU-rich RNA-binding proteins reportedly expressed in the pallium (Deschênes-Furry et al., 2006). Among them, Elavl2 was found to counter the *miR-9* suppression of luciferase expression from a reporter conjugated to the *Foxg1* 3′ UTR (Fig. 4*B*). This desuppression of *miR-9* activity by Elavl2 required the U-rich sequence located 5′ upstream of the *miR-9* responsive element in the

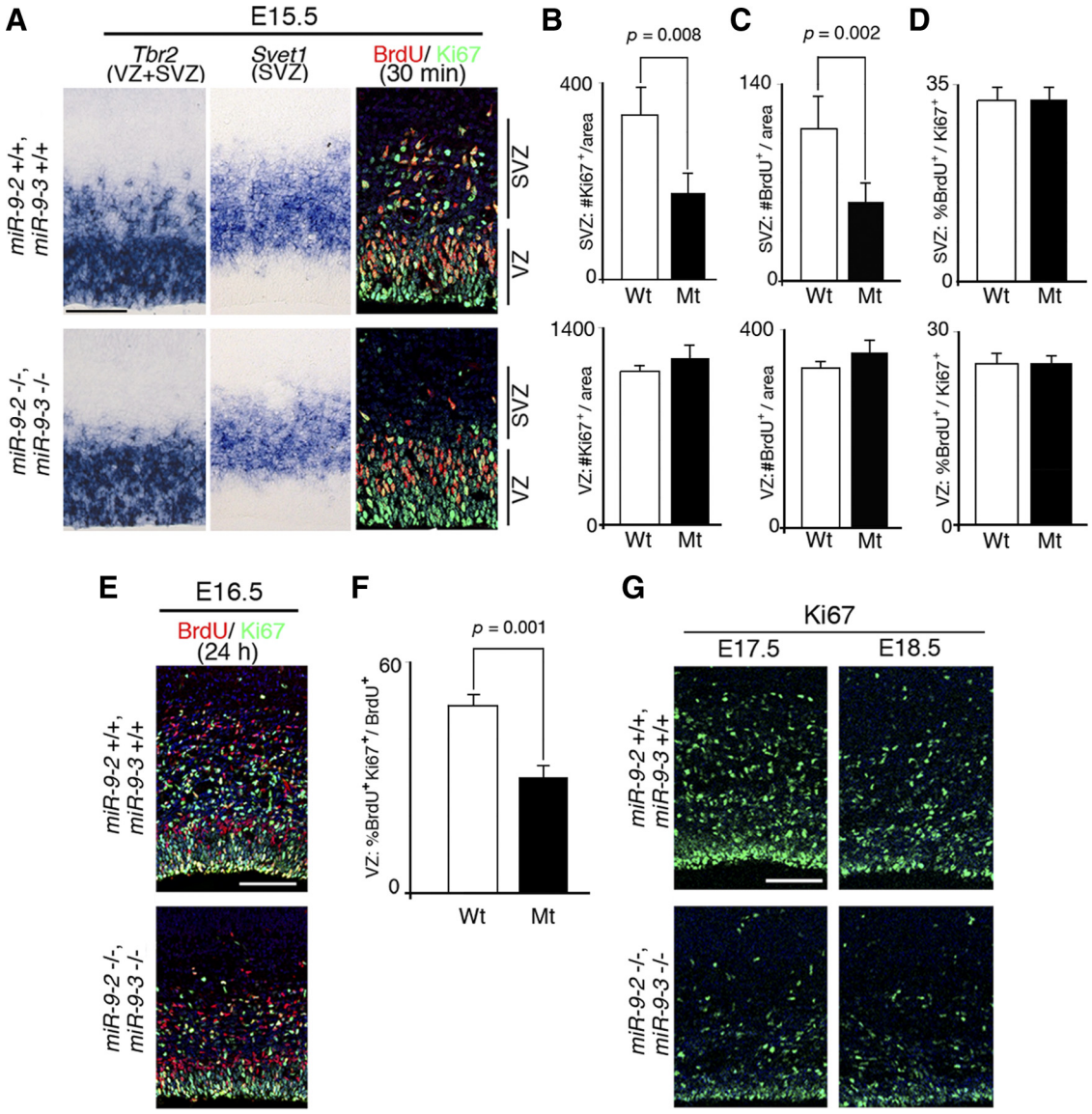

Figure 5. Progenitor proliferation in later *miR-9-2/3* double-mutant pallium. ***A***, Typical examples of RNA *in situ* hybridization of *Tbr2* and *Svet1* expression for the VZ and SVZ, and 30 min BrdU labeling and Ki67 staining for S phase and cycling cells in the pallium at E15.5, respectively. ***B***, ***C***, Quantification of Ki67-positive (***B***) and BrdU-positive (***C***) cells in the SVZ and VZ. ***D***, Cell cycle length as indicated by the number of BrdU and Ki67 double-positive cells among Ki67-positive cycling cells in the SVZ and VZ. ***E***, Typical examples of 24 h BrdU labeling and Ki67 staining for cells reentering the cell cycle in the VZ at E16.5. ***F***, Quantification of the cells reentering the cell cycle as the ratio of Ki67 and BrdU double-positive cells among BrdU-positive cells. ***G***, Typical examples of Ki-67 staining of E17.5 and E18.5 cortices. Quantification was performed as described in Materials and Methods. Scale bars: ***A***, ***E***, ***G***, 100 μm.

Foxg1 3′ UTR (Fig. 4*C*,*D*); *Foxg1* 3′ UTRs bearing mutations in the U-rich sequences (*Foxg1 3′ UTR MT1*, *MT2*, and *MT1 + 2*) were suppressed by *miR-9*, but these suppressions were not released by Elavl2. *Foxg1 3′ UTR MT1 + 2* completely lost the ability to be desuppressed by Elavl2. In addition, RNA affinity precipitation assay demonstrated that endogenous Elavl2 associates with *Foxg1 3′ UTR WT* RNA probe; the association was inefficient with the *Foxg1 3′ UTR MT1* probe (Fig. 4*E*). Furthermore, the Elavl2 overexpression in the dissociated cortical cells at E12.5 upregulated Foxg1 expression (Fig. 4*F*). *Elavl2* was expressed in the E16.5 VZ as well as the cortical plate and intermediate zone, but the expression was faint in the E14.5 VZ (Fig. 4*A*). These results suggest that Foxg1 expression is suppressed by *miR-9* at earlier stages, but the suppression is countered by Elavl2, whose expression increases at later stages. Concomitantly, no significant increase in the cycling Ki67-positive or BrdU-incorporated cells after 30 min of labeling was apparent in the *miR-9-2/3* double-mutant VZ at E15.5 as described below (Fig. 5*A–C*).

miR-9 enhances Nr2e1 and Pax6 expression, and progenitor proliferation was suppressed in later ventricular and subventricular zones

In P1 *miR-9-2/3* double mutant, cortical layers were hypoplastic (Fig. 1*E–J*). In E15.5 *miR-9-2/3* double-mutant pallium, the thickness of *Tbr2*-positive VZ (Tarabykin et al., 2001; Englund et al., 2005) was almost unaffected, whereas *Tbr2*- and *Svet1*-positive SVZ (Tarabykin et al., 2001) was reduced (Fig. 5*A*). The number of cycling Ki67-positive cells or of BrdU-positive S-phase cells was significantly reduced in the double-mutant SVZ (Fig. 5*B*,*C*). There was no significant difference in the ratio of BrdU-positive cells among Ki67-positive cells between wild-type and mutant SVZ (Fig. 5*D*), suggesting that IPCs in the mutant pallium had a cell cycle length similar to that of the wild type. We

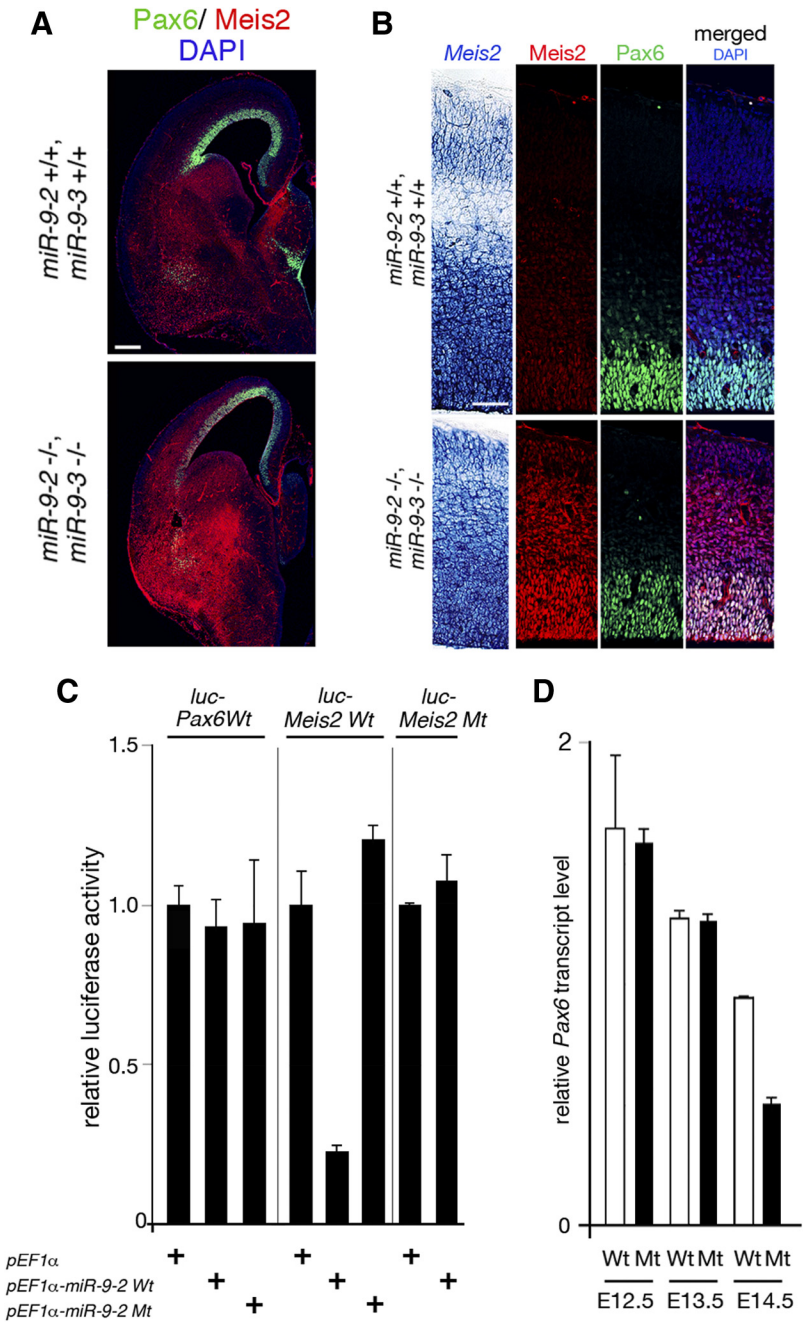

Figure 6. *miR-9* regulation of Pax6 expression. ***A***, Immunohistology of Pax6 (green) and Meis2 (red) protein expression in the E15.5 telencephalon. ***B***, RNA *in situ* hybridization of *Meis2* expression, anti-Meis2 or anti-Pax6 staining, and merged views of Meis2 and Pax6 protein expression with DAPI staining in the E15.5 pallium. ***C***, *miR-9-2* suppression of luciferase expression from a reporter conjugated to the wild-type and mutant *Pax6* and *Meis2* 3′ UTRs; in mutant *miR-9-2* (*miR-9-2Mt*), the mutation was introduced in the *miR-9* seed sequences. ***D***, Quantitative RT-PCR analyses of *Pax6* mRNA expression at indicated stages. Scale bars: ***A***, 200 μm; ***B***, 50 μm.

also examined cell cycle reentry in the VZ at E16.5 by labeling with BrdU for 24 h; the frequency of the cells reentering the cell cycle is given as the ratio of BrdU and Ki67 double-positive cells over the total number of BrdU-positive cells. This ratio was significantly reduced in the *miR-9-2/3* double-mutant VZ (Fig. 5*E*,*F*). Consistently, the number of Ki67-positive proliferating cells in the VZ significantly decreased at E17.5 and E18.5 (Fig. 5*G*), suggesting the depletion of the progenitor pool in the VZ at later stages.

Among genes suggested to regulate cortical progenitor proliferation and differentiation at later phases (see Introduction), *Id4*, *Pax6*, and *Nr2e1* mRNAs have *miR-9* target sequences (supplemental Fig. 3, available at www.jneurosci.org as supplemental material); none has *miR-9** responsive element. *miR-9-2* did not affect the luciferase expression from a reporter conjugated to the *Id4* 3′ UTR (Shibata et al., 2008); moreover, Id4 protein expression was almost unchanged in the *miR-9-2/3* double-mutant pallium (Fig. 3*M*,*N*). In contrast, Pax6 and Nr2e1 protein expressions were reduced in the E15.5 *miR-9-2/3* double mutants (Figs. 6*A*,*B*, 7*A*; Table 1). However, we were unable to demonstrate significant change of luciferase expression from a reporter conjugated to the *Pax6* 3′ UTR by *miR-9* (Fig. 6*C*). The *Pax6* mRNA expression reduces with telencephalon development (Fig. 6*D*). The double mutation did not affect the *Pax6* mRNA expression initially, but the reduction was more pronounced in the *miR-9-2/3* double-mutant telencephalon later than E14.5 (Fig. 6*D*). Meis2 has been known to suppress the *Pax6* expression (Agoston and Schulte, 2009), and *Meis2* mRNA has *miR-9* responsive element (supplemental Fig. 3, available at www.jneurosci.org as supplemental material). Indeed, wild-type *miR-9-2* suppressed luciferase expression from a reporter conjugated to the wild-type *Meis2* 3′ UTR, whereas mutant *miR-9-2* did not (Fig. 6*C*). Furthermore, *miR-9-2* did not suppress luciferase expression from a reporter conjugated to the *Meis2* 3′ UTR with a mutation in the *miR-9* responsive element (Fig. 6*C*). Meis2 protein expression was indeed enhanced in *miR-9-2/3* double-mutant pallium, although its expression was not significantly changed at the mRNA level (Fig. 6*A*,*B*; Table 1).

Nr2e1 expression was not significantly changed at the mRNA level (Fig. 7*B*), and *miR-9-2* did not suppress luciferase expression from a reporter conjugated to the *Nr2e1* 3′ UTR in P19 cells (Fig. 7*C*,*D*). It is reported that RNA-binding protein FXR1 activates protein expression from *miR369-3*-targeted tumor necrosis factor α mRNAs (Vasudevan et al., 2007). Among RNA-binding proteins expressed in the pallium (Deschênes-Furry et al., 2006), we found that Elavl1 (Ma et al., 1996) and Msi1 (Sakakibara et al., 1996) activated *miR-9-2*-directed luciferase expression from the reporter conjugated to the *Nr2e1* 3′ UTR. Neither Elavl1 nor Msi1 activated luciferase expression directed by mutant *miR-9-2* (Fig. 7*C*,*D*). Moreover, wild-type *miR-9-2*, but not mutant *miR-9-2*, upregulated the expression of endogenous Nr2e1 in P19 cells, synergistically with Elavl1 (Fig. 7*E*). Elavl1 did not relieve the *miR-9*-directed suppression of luciferase expression from the reporter conjugated to the *Foxg1* 3′ UTR (Fig. 4*B*), suggesting that the Elavl1 activity is specific to Nr2e1. *Elavl1* is expressed intensively in the VZ and moderately in the SVZ and cortical plate (data not shown); *Msi1* is expressed in the

VZ and SVZ (Sakakibara et al., 1996). *Msi1* enhanced the luciferase expression by itself (Fig. 7*D*). However, neither *Elavl1* nor *Msi1* mRNA has *miR-9* responsive elements, and their expressions were unchanged in the *miR-9-2/3* double-mutant telencephalon (Fig. 7*F*).

Neocortical lamination is malformed in miR-9-2/3 double mutants

Cajal-Retzius cells were significantly decreased but present (Fig. 3*A–F*), Nestin-positive radial glial fibers that function as substrates for radial neural migration were oriented normally (supplemental Fig. 5*A*, available at www.jneurosci.org as supplemental material), and inside-out lamination took place in the *miR-9-2/3* double-mutant neopallium. Concomitantly with the defects in progenitor proliferation and differentiation, however, cortical layers were hypoplastic in the P1 *miR-9-2/3* double mutants (Fig. 1*G*,*H*). At E18.5, *Foxp2*- or *Tbr1*-positive layer VI was almost normally generated, whereas calretinin-positive layer I, *Cux1*-positive layer II/III, *Satb2*-positive layer II-IV, *Rorβ*-positive layer IV, and calretinin-positive subplate were reduced (Fig. 8*A*). Normal generation of the layer VI was unexpected, because layer VI neurons are produced at approximately E12.5 (Langevin et al., 2007) when progenitor proliferation is enhanced in the double mutants. *Tbr1*-positive layer VI neurons as well as Tuj1- or *NeuroD1*-positive neurons were significantly reduced at E12.5 as described above (Fig. 3*M–T*). However, the layer VI neurons assessed by *Foxp2* transcript level were not significantly changed at E13.5 or E14.5 (Fig. 8*B*). Conversely, birthdating analysis also indicated that the number of BrdU-positive cells labeled at E14.5 was significantly decreased in mutant layer II–III, defined by *Cux1* expression at E18.5 (Fig. 8*C*). Notably, the *Er81*-positive layer V was also reduced, whereas Ctip2 expression was expanded into deeper layers in *miR-9-2/3* double mutants (Fig. 8*A*); *Er81* marks all layer V neurons, whereas Ctip2 marks corticospinal motor neurons (Molnár and Cheung, 2006). Moreover, the *Sox5* expression in V and VI layers was also decreased in the double mutants to approximately one-third of the wild-type level (Fig. 8*A*,*D*). Neither *Er81* nor *Ctip2* mRNAs have *miR-9* responsive elements. *Er81* is known to be a downstream target of Pax6 in cortical progenitors (Tuoc and Stoykova, 2008), and we speculate that the reduction of *Er81*-positive layer V is attributable to the Pax6 reduction. Sox5 is also known to suppress *Ctip2* expression in layer VI and the subplate (Kwan et al., 2008; Lai et al., 2008), and we assume that the expansion of Ctip2 expression is attributable to the *Sox5* reduction. However, *Sox5* mRNA does not have *miR-9* responsive element; thus, *miR-9* must enhance *Sox5* expression indirectly.

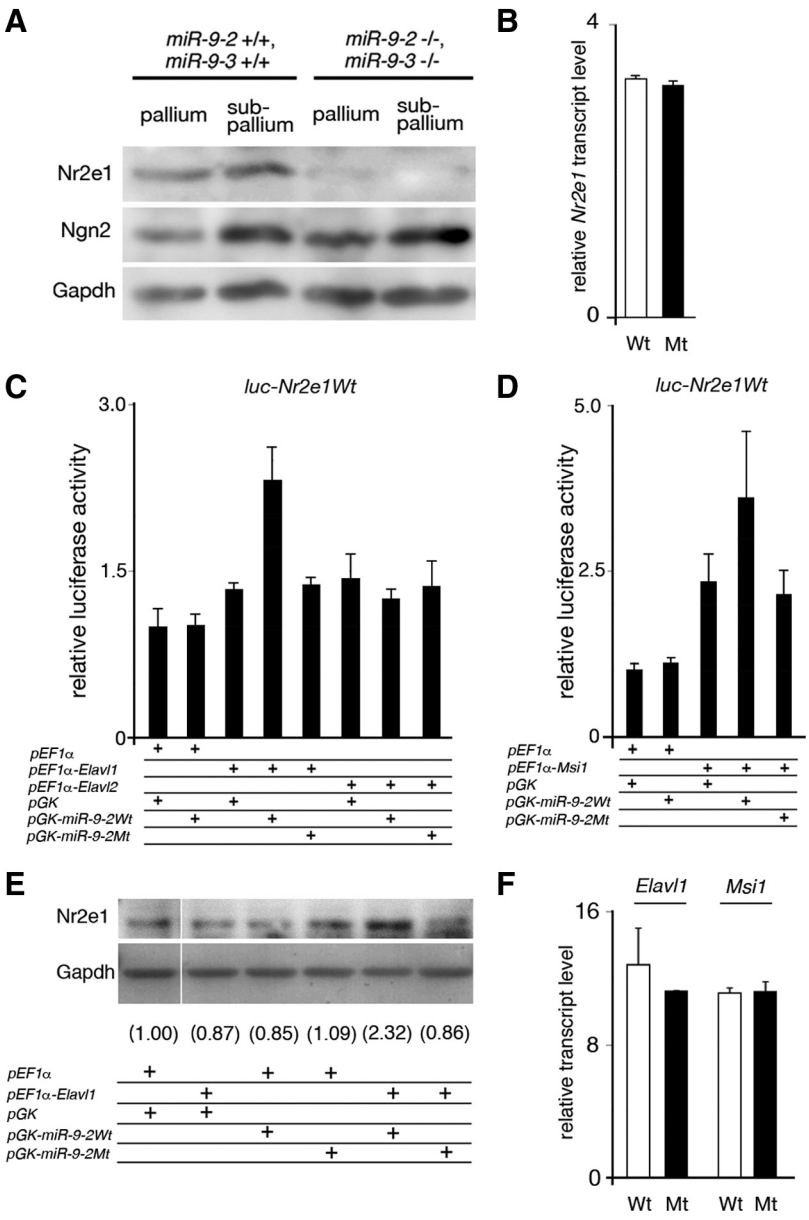

Figure 7. *miR-9* regulation of Nr2e1 expression. ***A***, Western blotting for Nr2e1 expression in E13.5 pallium and subpallium, with Ngn2 as a negative control and Gapdh as a loading control. ***B***, Quantitative RT-PCR for *Nr2e1* mRNA expression in cerebral hemispheres dissected at E16.5. ***C***, ***D***, Effects of *Elavl1* and *Elavl2* (***C***) and *Msi1* (***D***) on luciferase expression from a luciferase reporter conjugated to the *Nr2e1* 3′ UTR in P19 cells. No *miR-9* suppression of luciferase expression was observed from luciferase reporters conjugated to the 1.4 kb full-length *Nr2e1* 3′ UTR (***C***, ***D***) as used by Zhao et al. (2009) or with four tandem repeats of its 50 nt fragment containing *miR-9* responsive element (data not shown). ***E***, Increase in the endogenous Nr2e1 expression in P19 cells by Elavl1 and *miR-9*. P19 cells were transfected with *Elavl1* and/or *miR-9* expression vectors as indicated, and Nr2e1 expression was detected by Western blotting. Numerals give the relative intensity of each Nr2e1 band to that in control in which *pEF1α* and *pGK* vectors were transfected; each band intensity was normalized by the intensity of Gapdh band. ***F***, Quantitative RT-PCR analysis of *Elavl1* and *Msi1* mRNA expression in wild and *miR-9-2/3* double-mutant cortices at E16.5.

As expected from the malformation of cortical layers, each cortical projection was greatly reduced in the *miR-9-2/3* double mutants. Axons of commissural neurons labeled by L1 (corpus callosum, anterior commissure, and fornix/hippocampal commissure) were poorly formed (Fig. 8*E–J*), and corticofugal axons (CFAs) labeled by TAG-1 and L1 were also thin in the *miR-9-2/3* double-mutant pallium (see Fig. 10*A–D*′). Furthermore, the cortical interneurons that are born in the subpallium and tangentially

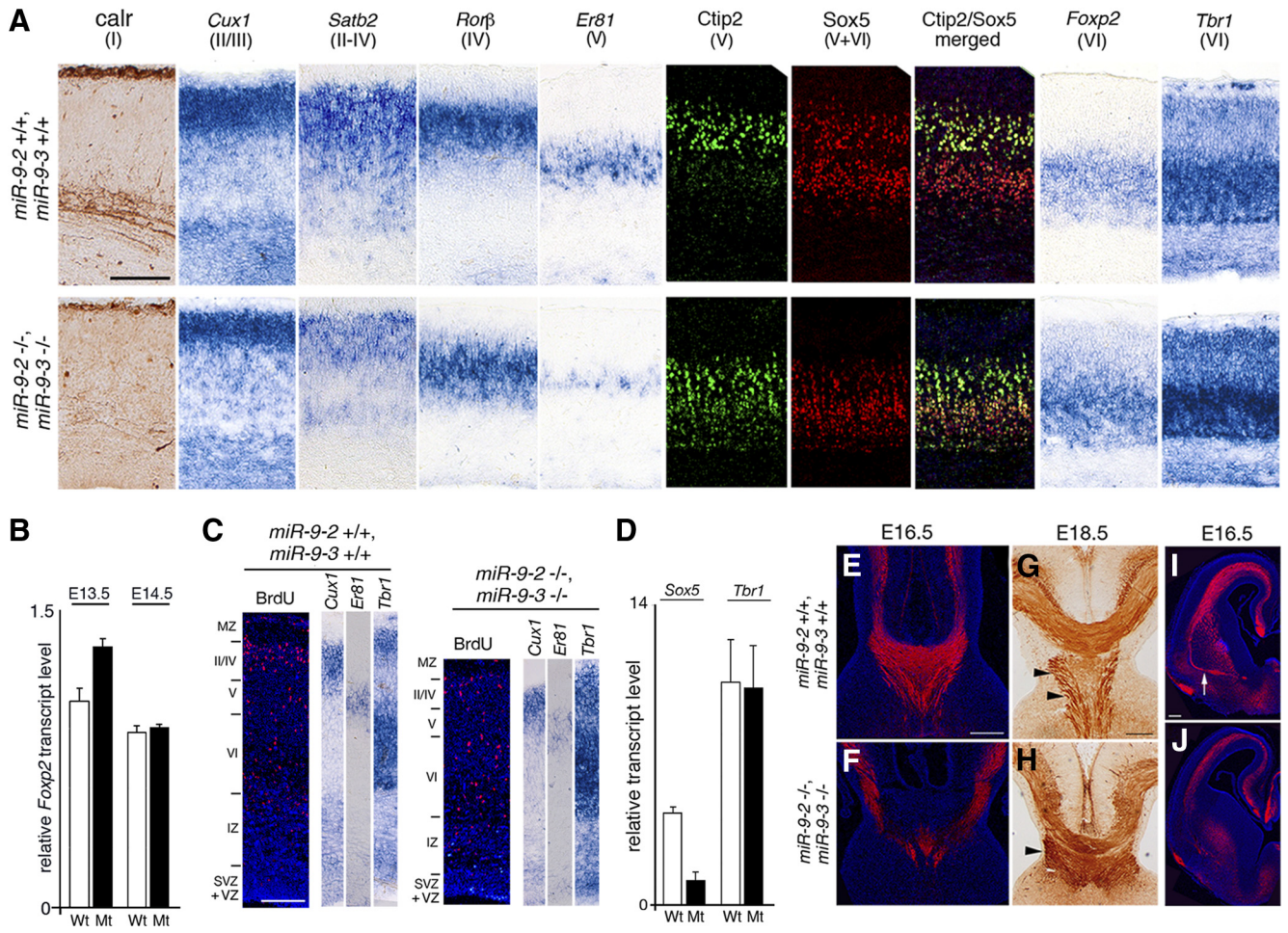

Figure 8. Layer formation in *miR-9-2/3* double-mutant neopallium. ***A***, Marker analysis for layer formation at E18.5. ***B***, Quantification of *Foxp2* mRNA expression at indicated stages. ***C***, Birthdating analysis of the E18.5 cortex by BrdU labeling at E14.5. ***D***, Quantitative RT-PCR analysis of *Sox5* and *Tbr1* mRNA expression in the pallium at E14.5. ***E–J***, Anti-L1 staining for corpus callosum, fornix/hippocampal commissure (arrowheads), and anterior commissure (arrow). Sections in ***E***, ***F***, ***I***, and ***J*** were immunostained as described in Materials and Methods, whereas the section in ***G*** and ***H*** was stained with 3,3′-diaminobenzidine tetrahydrochloride after immunoreaction with the secondary antibody conjugated to horseradish peroxidase. Scale bars: ***A***, ***E–J***, 200 μm; ***C***, 100 μm.

migrate into the pallium were scarcely present in the *miR-9-2/3* double-mutant pallium (supplemental Fig. 6*A–J*, available at www.jneurosci.org as supplemental material); this is coincident with the malformation of the intermediate and marginal zones that provide interneuron passages (Métin et al., 2006) or the reduction of TAG-1- or reelin-positive cells that guide the migration (Denaxa et al., 2001; Morante-Oria et al., 2003). However, interneurons were apparently normally specified in MGE (supplemental Fig. 6*K*,*L*, available at www.jneurosci.org as supplemental material). Moreover, interneurons in the rostral migratory stream to the olfactory bulb were also generated apparently normally in the *miR-9-2/3* double-mutant LGE (supplemental Fig. 6*M*,*N*, available at www.jneurosci.org as supplemental material).

miR-9 suppresses Gsh2 and Foxg1 expression and progenitor proliferation is enhanced in the miR-9-2/3 double-mutant subpallium

Morphologically, the *miR-9-2/3* double-mutant subpallium was almost normal at E12.5 (Fig. 3*A–H*,*K–N*) (data not shown) but hyperplastic at E15.5; the cell-dense proliferating field was markedly expanded into the deep differentiating field (Figs. 1*E*,*F*, 9*A*,*B*). Indeed, the Brn2- and *Mash1*-positive fields expanded deeply in the *miR-9-2/3* double-mutant subpallium (Fig. 9*C*,*D*, *C*″,*D*″,*E*,*F*). Concomitantly, the Ctip2-, *Lmo4*-, and *Foxp1*-positive differentiating field (Hermanson et al., 1999; Tamura et al., 2004; Arlotta et al., 2008) was greatly reduced (Fig. 9*C*′–*D*″,*G–J*). The *Islet1*-positive LGE SVZ (Stenman et al., 2003a) was also markedly expanded, whereas that in the differentiating area was reduced (Fig. 9*K*,*L*). At E15.5, the number of BrdU-positive and Ki67-positive cells in the lateral ganglionic eminences was increased in the *miR-9-2/3* double-mutant LGE (Fig. 9*M–P*), particularly in the deeper area. However, such hyperproliferation was not apparent at E12.5 (supplemental Fig. 7*A–F*, available at www.jneurosci.org as supplemental material).

Among genes reported to be essential to progenitor cell proliferation in the VZ and SVZ of ganglionic eminences (see Introduction), we found none has *miR-9** responsive element, and neither *Mash1*, *Dlx1/2/5/6*, nor *Nkx2.1* has *miR-9* responsive element. *Gsh2* mRNA, however, has *miR-9* responsive element in its 3′ UTRs (supplemental Fig. 3, available at www.jneurosci.org as supplemental material). Wild-type *miR-9-2* effectively suppressed the expression of luciferase from a reporter conjugated to the wild-type *Gsh2* 3′ UTR but not the 3′ UTR, of which the *miR-9* responsive element was transversely mutated (Fig. 9*Q*). Gsh2 protein level was indeed enhanced in the *miR-9-2/3* double-mutant compared with the wild-type subpallial region (Fig. 9*R*,*S*; Table 1). In addition, Gsh2 overexpression in the LGE region by electroporation markedly enhanced the number of Ki67-positive

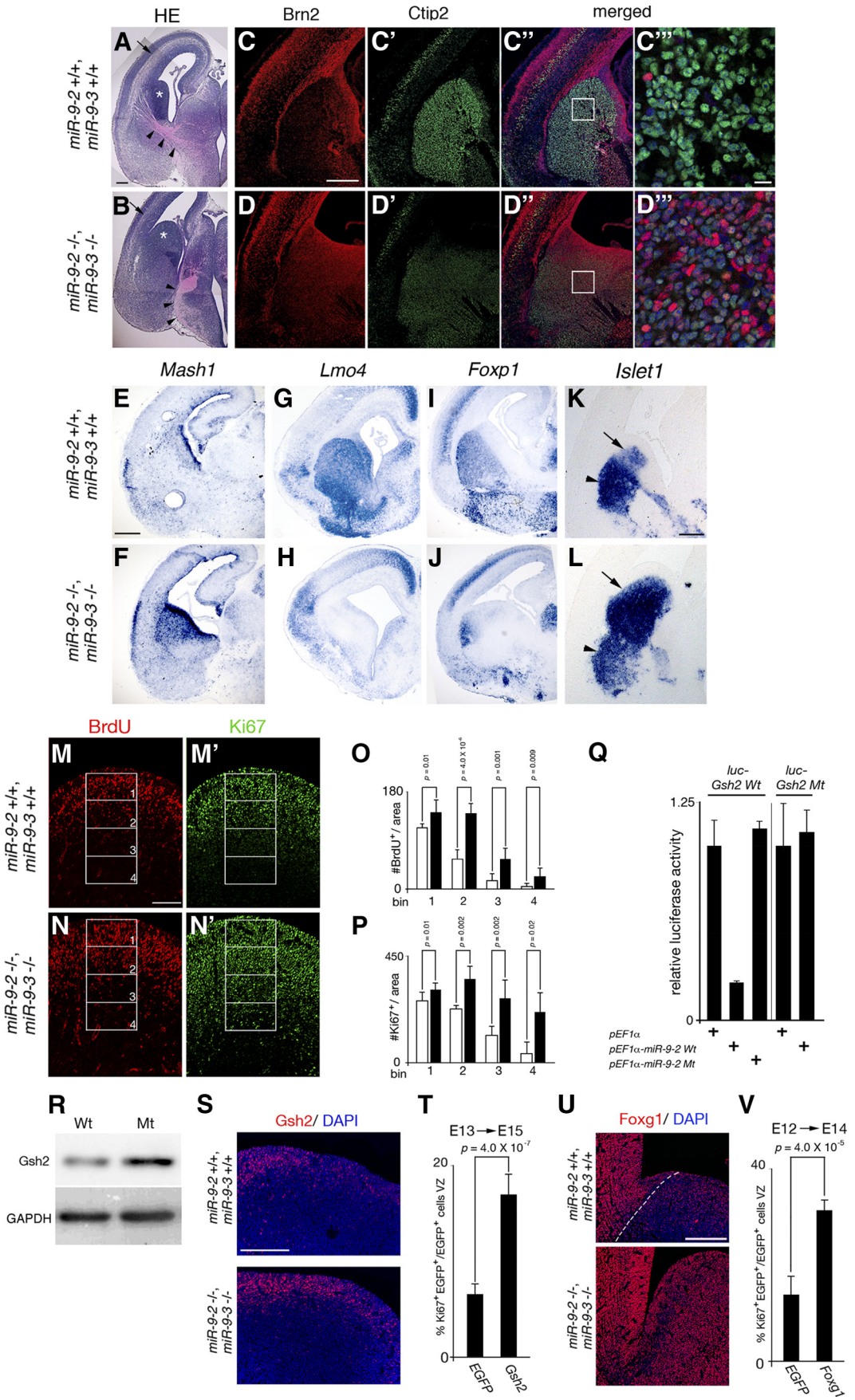

Figure 9. *miR-9* regulation of cell proliferation and neural differentiation in the subpallium. ***A***, ***B***, Coronal sections of the E15.5 telencephalon stained with hematoxylin/eosin. Arrowheads indicate TCA trajectories, and arrows the intermediate zones. ***C***, ***D***, Anti-Brn2 staining of the E18.5 subpallium for the proliferative zone. ***C'***, ***D'***, Anti-Ctip2 staining for the (*Figure legend continues*.)

cells (Fig. 9*T*). Foxg1 is also expressed in subpallium, but its role in subpallial progenitor proliferation and differentiation has been unclear in *Foxg1* mutants because of the earlier defect in the subpallial specification (Martynoga et al., 2005; Manuel et al., 2010). Foxg1 protein expression was modest in the E15.5 wild-type subpallium but enhanced in the *miR-9-2/3* double-mutant subpallium (Fig. 9*U*); this increase was not apparent in the E12.5 *miR-9-2/3* double-mutant subpallium (supplemental Fig. 7*G*,*H*, available at www.jneurosci.org as supplemental material). In addition, Foxg1 overexpression enhanced the proportion of cycling cells in the subpallium (Fig. 9*V*).

Dorsal shift of pallial–subpallial boundary

The PSB is proposed to be determined by the counteraction of Pax6 and Gsh2 (Toresson et al., 2000; Yun et al., 2001). The PSB also shifts dorsally in *Nr2e1* mutants (Stenman et al., 2003b). Consistent with the reduction of Pax6 and Nr2e1 expression and the increase of Gsh2 expression in the *miR-9-2/3* double mutants, the *Tbr2/Gsh2* boundary that marks the PSB shifted dorsally and coincided with the morphological flexure between the pallium and subpallium (supplemental Fig. 8*A–D*, available at www.jneurosci.org as supplemental material). The PSB is also marked morphologically by a fasciculated palisade of radial glial fibers (Stenman et al., 2003b). In *miR-9-2/3* double mutants, the Nestin-positive glial palisade was aberrant and less fasciculated (supplemental Fig. 8*E*,*F*, available at www.jneurosci.org as supplemental material). With the dorsal shift of the PSB, the *Dbx1*-positive ventral pallium that juxtaposes to the PSB was greatly reduced as stated above (Fig. 3*K*,*L*), and *Er81*-positive basolateral amygdala that derives from the pallium (Stenman et al., 2003b) was lost in the *miR-9-2/3* double mutants (supplemental Fig. 8*G*,*H*, available at www.jneurosci.org as supplemental material).

Thalamocortical axon and CFA projections are misrouted with corridor malformation in MGE

In the *miR-9-2/3* double-mutant ventral telencephalon, CFAs poorly innervated the internal capsule (Fig. 10*A–D′*). Thalamocortical axons (TCAs) labeled by L1 and GAP43 were nearly lost before reaching the internal capsule, and a majority of fibers abnormally descended into the hypothalamus (Figs. 9*A*,*B*, 10*A–D′*). *Islet1*- and *Meis2*-positive corridor neurons, which originate from the LGE and locate between the *Nkx2.1*-positive proliferating zone and globus pallidus (López-Bendito et al., 2006) (Fig. 10*E*,*E′*,*G*,*G′*), are known to function as a gateway for TCA tracts to the internal capsule. *Nkx2.1*-positive globus pallidus was nearly lost (Fig. 10*E–H*), and *Islet1*- and *Meis2*-positive corridor neurons were expanded or dispersed in the *miR-9-2/3* double mutants (Fig. 10*E′*,*F′*,*G′*,*H′*). In a mutant that has no *Pax6* expression in the ventral telencephalon, the corridor cells are dispersed and TCA is not trajected into the telencephalon (Simpson et al., 2009). This *Pax6* expression was, however, not significantly altered in the *miR-9-2/3* double mutant at E15.5 (Fig. 10*I*,*J*). Not only *Meis2*, as described above, but also *Islet1* mRNA has *miR-9* responsive elements (supplemental Fig. 3, available at www.jneurosci.org as supplemental material). Meis2 protein level was increased in the *miR-9-2/3* double-mutant subpallium (Fig. 6*A*,*B*). Wild-type *miR-9-2* moderately suppressed luciferase expression from a reporter conjugated to the *Islet1* 3′ UTR (Fig. 10*K*). The increase in Islet1 protein expression was also moderate in the *miR-9-2/3* double-mutant subpallium (Fig. 10*L*; Table 1).

Discussion

The *miR-9-2/3* double mutants demonstrate that *miR-9* orchestrates neurogenesis in the pallium and subpallium by regulating the expression of multiple genes that function in progenitor proliferation and differentiation. Furthermore, we propose that these *miR-9* functions are modulated by the RNA-binding proteins. Increase in Foxg1 expression in *miR-9-2/3* double mutant at early neurogenic stages is consistent with the reduction in Cajal-Retzius cells and early-born neurons (Dou et al., 1999; Hanashima et al., 2002, 2004; Martynoga et al., 2005; Muzio and Mallamaci, 2005). Nr2e1 and Pax6 reduction is also consistent with the decrease in later progenitor proliferation in pallium (Stenman et al., 2003b; Roy et al., 2004; Schuurmans et al., 2004) and the increase in Gsh2 and Foxg1 expression with the increase in progenitor proliferation in subpallium (Toresson et al., 2000; Yun et al., 2001) in this study. However, the Foxg1 increase was at a twofold level, and it is a question whether this level of Foxg1 increase can fully explain the reduction of Cajal-Retzius cells and early-born neurons; the question remains for future studies such as Foxg1 overexpression or the *miR-9-2/3* compound mutation with heterozygous *Foxg1* mutation. It should also be examined whether and how *Nr2e1* or *Pax6* overexpression can restore the later pallium phenotype in the *miR-9-2/3* double mutants. Gsh2 increase in the *miR-9-2/3* double mutants was also ~1.7-fold and Islet1 increase was ~1.4-fold. It is plausible that *miR-9* targets many more genes in each event. The *miR-9* regulation of each gene is moderate, and the regulation of a single gene by *miR-9* might not be responsible in each phenotype; rather, *miR-9* mutant phenotype might be explained by the cumulation of the moderate reduction of multiple genes that participate in an event.

Previous studies (Bhattacharyya et al., 2006; Kedde et al., 2007; Vasudevan and Steitz, 2007; Vasudevan et al., 2007) and this study strongly suggest that it depends on the context of RNA-binding proteins expressed whether a microRNA suppresses or enhances the protein expression or has no effect. The *Foxg1* 3′ UTR has U-rich sequences, and this study proposes that the *miR-9* suppression of Foxg1 protein expression is countered by an AU-rich RNA binding protein, Elavl2, later than E15.5. We also propose that *miR-9* targets *Nr2e1* mRNA to enhance its pro-

←

(*Figure legend continued.*) striatal neurons in the adjacent sections. ***C″***, ***D″***, Their merged views. ***C‴***, ***D‴***, The enlarged views of the regions boxed in ***C″***, ***D″***. ***E–L***, RNA *in situ* hybridization of *Mash1* (***E***, ***F***) expression for the proliferative zone at E17.5, of *Lmo4* (***G***, ***H***) and *Foxp1* (***I***, ***J***) expression for the striatal neurons at E17.5, and of *Islet1* (***K***, ***L***) expression for striatal neurons (arrowheads) and SVZ (arrows) at E15.5. ***M–N′***, Typical examples of 30 min BrdU labeling for S-phase cells (***M***, ***N***) and Ki67 staining for cycling cells (***M′***, ***N′***) in the E15.5 LGE. ***O***, ***P***, The number of BrdU-positive (***O***) and Ki67-positive (***P***) cells in the four bins along the ventricular–pial axis of the LGE shown in ***M–N′***. Quantification was performed as described in Materials and Methods. ***Q***, Luciferase expression from a luciferase reporter conjugated to the wild-type and mutant *Gsh2* 3′ UTR: the mutation was introduced in the *miR-9* responsive element. ***R***, Western blotting for Gsh2 expression in cerebral hemispheres at E15.5. Quantification of the Gsh2 protein level by normalizing with Gapdh levels (loading control) indicated 1.7-fold increase in *miR-9-2/3* double-mutant telencephalon. ***S***, Anti-Gsh2 staining in the wild-type and double-mutant E15.5 LGE region. ***T***, ***V***, The effects of *Gsh2* (***T***) and *Foxg1* (***V***) overexpression by *exo utero* electroporation at E13 or E12 on cell proliferation in the subpallium at E15 or E14, respectively. The percentage of Ki67 and EGFP double-positive cells among total EGFP-positive cells is indicated. Quantification was performed as described in Materials and Methods. ***U***, Anti-Foxg1 staining in the wild-type and *miR-9-2/3* double-mutant E15.5 LGE region. ***A–L***, ***M–N′***, ***S***, and ***U*** are all coronal views. Nr2e1 is known to promote cell proliferation in subpallium (Stenman et al., 2003c), and thus the reduction in Nr2e1 expression in E15.5 *miR-9-2/3* double-mutant subpallium (Fig. 7*A*) cannot account for the hyperproliferation of progenitors in the *miR-9-2/3* double-mutant subpallium. The areas of each bin in (***M–N′***) are 180 × 100 μm. Scale bars: ***A***, ***B***, ***M–N′***, 100 μm; ***C–D″***, ***E–L***, 300 μm; ***C‴***, ***D‴***, 10 μm; ***S***, ***U***, 200 μm.

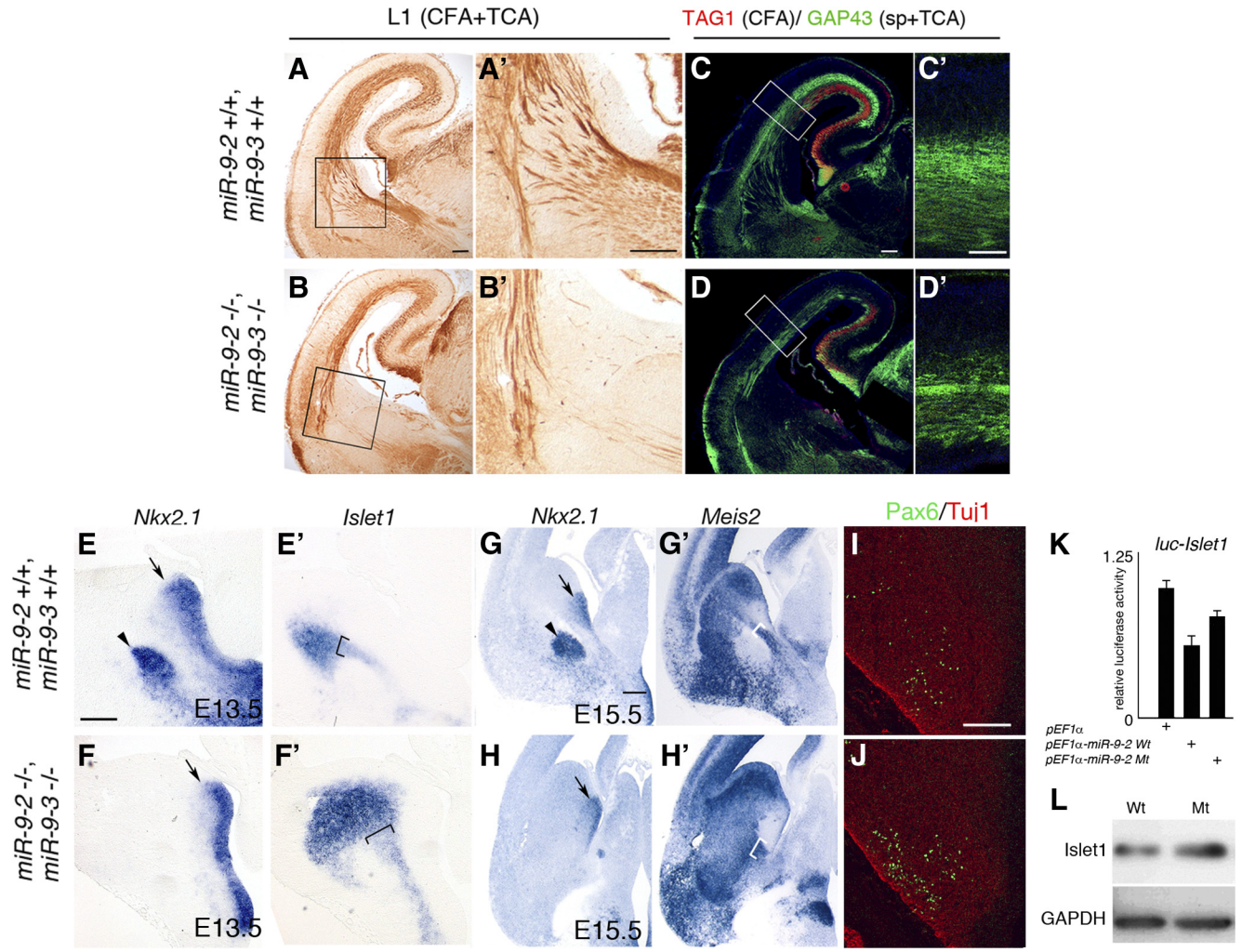

Figure 10. Corticofugal and thalamocortical projections with corridor malformation in *miR-9-2/3* double-mutant subpallium. ***A***, ***B***, Anti-L1 staining for CFAs and TCAs at E18.5. ***A′***, ***B′***, Enlarged views of the internal capsule areas boxed in ***A*** and ***B***. ***C***, ***D***, Anti-TAG1 (red) and anti-GAP43 (green) staining for CFAs and TCAs/subplate at E18.5. ***C′***, ***D′***, Enlarged views of the areas boxed in ***C*** and ***D***. Scale bars: ***A–D***, 100 μm; ***C′***, ***D′***, 50 μm. RNA *in situ* hybridization of *Nkx2.1* for the proliferating field of the MGE and globus pallidus at E13.5 (***E***, ***F***), of *Islet1* for corridor in sections adjacent to ***E*** and ***F*** (***E′***,***F′***), and of *Nkx2.1* (***G***, ***H***) and *Meis2* (***G′***, ***H′***) for the ventral telencephalon in adjacent sections at E15.5. ***I***, ***J***, Anti-Pax6 (green) and Tuj1 (red) staining in the E15.5 subpallium. Arrowheads indicate the globus pallidus in ***E*** and ***G***; arrows indicate the MGE VZ in ***E–H***, and brackets indicate the corridor in ***E′–H′***. Scale bars: ***E–F′***, 50 μm; ***G–H′***, 200 μm; ***I***, ***J***, 100 μm. ***K***, *miR-9-2* suppression of luciferase expression from a reporter conjugated to the *Islet1* 3′ UTR. ***L***, Moderate increase of Islet1 expression in E13.5 *miR-9-2/3* double-mutant cerebral hemispheres.

tein expression in cooperation with Elavl1 and/or Msi1. Notably, *miR-9* suppresses the expression of luciferase conjugated to the 1.4 kb *Nr2e1* 3′ UTR in HEK 293 cells and adult neural stem cells (Zhao et al., 2009). We speculate that the discrepancy is explained by differences in cell types or RNA binding protein repertoires. Extensive analysis of factors that bind to *Foxg1* and *Nr2e1* 3′ UTRs site and stage specifically are required to clarify the precise mechanisms of the *miR-9* regulation of Foxg1 and Nr2e1 expression. *miR-9* was ineffective on *Id4* and *Pax6* 3′ UTRs and only marginally effective on *Islet1* 3′ UTR in the luciferase assay with the P19 cells. However, *miR-9* might also target these mRNAs efficiently *in vivo* in the presence of RNA binding proteins that are missing or insufficient in the P19 cells. At the same time, the possibility that *miR-9* enhances Nr2e1 expression indirectly by suppressing a gene that inhibits *Nr2e1* expression cannot be ruled out. This possibility will be tested in future studies by deleting the *miR-9* responsive element in endogenous *Nr2e1*; *Nr2e1* expression from such allele should not be affected by *miR-9-2/3* deficiency if *miR-9* directly targets Nr2e1.

Cajal-Retzius cells are reduced in *miR-9-2/3* double mutants as expected from our previous study (Shibata et al., 2008). However, a significant number of Cajal-Retzius cells remain in the *miR-9-2/3* double mutants, explaining the normal lamination in the inside-out pattern (Yoshida et al., 2006). The presence of *miR-9-1* in the *miR-9-2/3* double mutants might explain the incomplete loss of Cajal-Retzius cells (Fig. 3*A–F*). Alternatively, microRNAs fine-tune protein expression levels rather than completely switching gene expression on and off, and a significant number of Cajal-Retzius cells might be generated even if *miR-9* were completely lost. This must await the analyses of *miR-9-1/2/3* triple mutants, and the issue must be kept in mind in interpreting all phenotypes of *miR-9-2/3* double mutants.

We propose that *miR-9* targets *Meis2* in both pallium and subpallium, but the roles of Meis2 in telencephalon development remain to be demonstrated. The mechanisms of the *Meis2*- and *Islet-1*-positive corridor expansion, including whether it is a real expansion or dispersion brought about by the loss of *Nkx2–1*-positive globus pallidus, and the significance of the corridor abnormality in TCA projection require additional studies. No reduction of corridor was reported in *Islet1* knock-out mutants (Elshatory and Gan, 2008), but the effects of Islet1 overexpression

in the corridor formation remain to be determined. The reduction of differentiating field in subpallium but normal differentiation of interneurons as well as details of the lack of tangential migration of interneurons in *miR-9-2/3* double mutants also require additional study; reduction in striatum differentiation but normal interneuron generation was observed in *Nr2e1* mutant LGE (Stenman et al., 2003c). The reason why the layer VI was apparently normal in the double mutants, against the increase in progenitor proliferation and decrease in neuronal differentiation at E12.5, remains uncertain; layer VI neuron production was caught up at E13.5 in *miR-9-2/3* double mutants. To explain this, the origin of layer VI neurons or the birthdate analysis of double-mutant progenitor cells must first be examined in detail during E12.5–E13.5. *miR-9** expression was decreased to 38% in *miR-9-2/3* double-mutant telencephalon at E16.5, but this study could not demonstrate *miR-9** functions in neurogenesis in telencephalon. More detailed studies are required to assess *miR-9** regulation of REST, CoREST, and BAF53a expression; it might be stage- and/or site-dependent in terms of RNA binding partners. In addition, we could not find other *miR-9** target candidates with the criteria described in the previous paper (Shibata et al., 2008). The criteria include the conservation of *miR-9** responsive element among mouse, human, and chick orthologs, and the analyses of genes that conserve *miR-9/miR-9** responsive elements between mouse and human orthologs may be desired. A lot of questions remain to future studies. Nevertheless, the study fully demonstrates that *miR-9* is a crucial regulator of progenitor proliferation in both the pallium and subpallium through the regulation of multiple genes.

Finally, defects in subpallial development in the *miR-9-2/3* double mutant are reminiscent of mutant mice in which exon 1 of huntingtin (*Htt*) was replaced with a human mutant *Htt* exon 1; progenitor proliferation is enhanced, and differentiation suppressed, in the striatum (Molero et al., 2009). Huntington's disease is a neurogenic disorder associated with dysfunction and degeneration of mainly medial spiny neurons of the striatum, having a midlife onset. However, the nexus of Huntington's disease might occur at an earlier time in the specification of the neurons (Molero et al., 2009). Nuclear localization of REST by *Htt* mutation with an expanded polyglutamate stretch is one putative molecular mechanism underlying Huntington's disease pathogenesis (Zuccato et al., 2003). REST suppresses the transcription of neuron restrictive silencer element-controlled neural genes. *miR-9/miR-9** is reported to suppress REST and CoREST expression *in vitro* (Packer et al., 2008) and REST in turn to suppress *miR-9* expression for progenitor proliferation (Conaco et al., 2006). Furthermore, *miR-9/9** expression was significantly decreased in Huntington's disease patient cortices (Packer et al., 2008). *In vivo* functions of REST in neurogenesis in mouse telencephalon have been not demonstrated, and REST expression was not significantly altered in *miR-9-2/3* double-mutant E13.5 telencephalon. However, more detailed analysis, especially on *miR-9-1/2/3* triple mutants, is worthwhile to elucidate the significance of *miR-9/miR-9** functions in the neurogenesis as well as in the pathological mechanisms of Huntington's disease.

References

Abramoff MD, Magelhaes PJ, Ram SJ (2004) Image processing with ImageJ. Biophotonics Int 11:36–42.

Agoston Z, Schulte D (2009) Meis2 competes with the Groucho co-repressor Tle4 for binding to Otx2 and specifies tectal fate without induction of a secondary midbrain-hindbrain boundary organizer. Development 136:3311–3322.

Anderson SA, Qiu M, Bulfone A, Eisenstat DD, Meneses J, Pedersen R, Rubenstein JL (1997) Mutations of the homeobox genes Dlx-1 and Dlx-2 disrupt the striatal subventricular zone and differentiation of late born striatal neurons. Neuron 19:27–37.

Arlotta P, Molyneaux BJ, Jabaudon D, Yoshida Y, Macklis JD (2008) Ctip2 controls the differentiation of medium spiny neurons and the establishment of the cellular architecture of the striatum. J Neurosci 28:622–632.

Bartel DP (2009) MicroRNAs: target recognition and regulatory functions. Cell 136:215–233.

Bedford L, Walker R, Kondo T, van Crüchten I, King ER, Sablitzky F (2005) Id4 is required for the correct timing of neural differentiation. Dev Biol 280:386–395.

Bhattacharyya SN, Habermacher R, Martine U, Closs EI, Filipowicz W (2006) Relief of microRNA-mediated translational repression in human cells subjected to stress. Cell 125:1111–1124.

Carninci P, Kasukawa T, Katayama S, Gough J, Frith MC, Maeda N, Oyama R, Ravasi T, Lenhard B, Wells C, Kodzius R, Shimokawa K, Bajic VB, Brenner SE, Batalov S, Forrest AR, Zavolan M, Davis MJ, Wilming LG, Aidinis V, et al. (2005) The transcriptional landscape of the mammalian genome. Science 309:1559–1563.

Conaco C, Otto S, Han JJ, Mandel G (2006) Reciprocal actions of REST and a microRNA promote neuronal identity. Proc Natl Acad Sci U S A 103:2422–2427.

De Pietri Tonelli D, Pulvers JN, Haffner C, Murchison EP, Hannon GJ, Huttner WB (2008) miRNAs are essential for survival and differentiation of newborn neurons but not for expansion of neural progenitors during early neurogenesis in the mouse embryonic neocortex. Development 135:3911–3921.

Delaloy C, Liu L, Lee JA, Su H, Shen F, Yang GY, Young WL, Ivey KN, Gao FB (2010) MicroRNA-9 coordinates proliferation and migration of human embryonic stem cell-derived neural progenitors. Cell Stem Cell 6:323–335.

Denaxa M, Chan CH, Schachner M, Parnavelas JG, Karagogeos D (2001) The adhesion molecule TAG-1 mediates the migration of cortical interneurons from the ganglionic eminence along the corticofugal fiber system. Development 128:4635–4644.

Deschênes-Furry J, Perrone-Bizzozero N, Jasmin BJ (2006) The RNA-binding protein HuD: a regulator of neuronal differentiation, maintenance and plasticity. Bioessays 28:822–833.

Dou CL, Li S, Lai E (1999) Dual role of brain factor-1 in regulating growth and patterning of the cerebral hemispheres. Cereb Cortex 9:543–550.

Elshatory Y, Gan L (2008) The LIM-homeobox gene Islet-1 is required for the development of restricted forebrain cholinergic neurons. J Neurosci 28:3291–3297.

Englund C, Fink A, Lau C, Pham D, Daza RA, Bulfone A, Kowalczyk T, Hevner RF (2005) Pax6, Tbr2, and Tbr1 are expressed sequentially by radial glia, intermediate progenitor cells, and postmitotic neurons in developing neocortex. J Neurosci 25:247–251.

Flames N, Pla R, Gelman DM, Rubenstein JL, Puelles L, Marín O (2007) Delineation of multiple subpallial progenitor domains by the combinatorial expression of transcriptional codes. J Neurosci 27:9682–9695.

Griffiths-Jones S (2006) miRBase: the microRNA sequence database. Methods Mol Biol 342:129–138.

Guillemot F, Molnár Z, Tarabykin V, Stoykova A (2006) Molecular mechanisms of cortical differentiation. Eur J Neurosci 23:857–868.

Hanashima C, Shen L, Li SC, Lai E (2002) Brain factor-1 controls the proliferation and differentiation of neocortical progenitor cells through independent mechanisms. J Neurosci 22:6526–6536.

Hanashima C, Li SC, Shen L, Lai E, Fishell G (2004) Foxg1 suppresses early cortical cell fate. Science 303:56–59.

Hanashima C, Fernandes M, Hebert JM, Fishell G (2007) The role of Foxg1 and dorsal midline signaling in the generation of Cajal-Retzius subtypes. J Neurosci 27:11103–11111.

Hermanson O, Sugihara TM, Andersen B (1999) Expression of LMO-4 in the central nervous system of the embryonic and adult mouse. Cell Mol Biol 45:677–686.

Horton S, Meredith A, Richardson JA, Johnson JE (1999) Correct coordination of neuronal differentiation events in ventral forebrain requires the bHLH factor MASH1. Mol Cell Neurosci 14:355–369.

Huang Z (2009) Molecular regulation of neuronal migration during neocortical development. Mol Cell Neurosci 42:11–22.

Kedde M, Strasser MJ, Boldajipour B, Oude Vrielink JA, Slanchev K, le Sage C, Nagel R, Voorhoeve PM, van Duijse J, Ørom UA, Lund AH, Perrakis A, Raz E, Agami R (2007) RNA-binding protein Dnd1 inhibits microRNA access to target mRNA. Cell 131:1273–1286.

Kloosterman WP, Wienholds E, de Bruijn E, Kauppinen S, Plasterk RH (2006) In situ detection of miRNAs in animal embryos using LNA-modified oligonucleotide probes. Nat Methods 3:27–29.

Kwan KY, Lam MM, Krsnik Z, Kawasawa YI, Lefebvre V, Sestan N (2008) SOX5 postmitotically regulates migration, postmigratory differentiation, and projections of subplate and deep-layer neocortical neurons. Proc Natl Acad Sci U S A 105:16021–16026.

Lagos-Quintana M, Rauhut R, Yalcin A, Meyer J, Lendeckel W, Tuschl T (2002) Identification of tissue-specific microRNAs from mouse. Curr Biol 12:735–739.

Lai T, Jabaudon D, Molyneaux BJ, Azim E, Arlotta P, Menezes JR, Macklis JD (2008) SOX5 controls the sequential generation of distinct corticofugal neuron subtypes. Neuron 57:232–247.

Langevin LM, Mattar P, Scardigli R, Roussigné M, Logan C, Blader P, Schuurmans C (2007) Validating in utero electroporation for the rapid analysis of gene regulatory elements in the murine telencephalon. Dev Dyn 236:1273–1286.

Leucht C, Stigloher C, Wizenmann A, Klafke R, Folchert A, Bally-Cuif L (2008) MicroRNA-9 directs late organizer activity of the midbrain-hindbrain boundary. Nat Neurosci 11:641–648.

López-Bendito G, Cautinat A, Sánchez JA, Bielle F, Flames N, Garratt AN, Talmage DA, Role LW, Charnay P, Marín O, Garel S (2006) Tangential neuronal migration controls axon guidance: a role for neuregulin-1 in thalamocortical axon navigation. Cell 125:127–142.

Ma WJ, Cheng S, Campbell C, Wright A, Furneaux H (1996) Cloning and characterization of HuR, a ubiquitously expressed Elav-like protein. J Biol Chem 271:8144–8151.

Manuel M, Martynoga B, Yu T, West JD, Mason JO, Price DJ (2010) The transcription factor Foxg1 regulates the competence of telencephalic cells to adopt subpallial fates in mice. Development 137:487–497.

Martynoga B, Morrison H, Price DJ, Mason JO (2005) Foxg1 is required for specification of ventral telencephalon and region-specific regulation of dorsal telencephalic precursor proliferation and apoptosis. Dev Biol 283:113–127.

Métin C, Baudoin JP, Rakić S, Parnavelas JG (2006) Cell and molecular mechanisms involved in the migration of cortical interneurons. Eur J Neurosci 23:894–900.

Molero AE, Gokhan S, Gonzalez S, Feig JL, Alexandre LC, Mehler MF (2009) Impairment of developmental stem cell-mediated striatal neurogenesis and pluripotency genes in a knock-in model of Huntington's disease. Proc Natl Acad Sci U S A 106:21900–21905.

Molnár Z, Cheung AF (2006) Towards the classification of subpopulations of layer V pyramidal projection neurons. Neurosci Res 55:105–115.

Molyneaux BJ, Arlotta P, Menezes JR, Macklis JD (2007) Neuronal subtype specification in the cerebral cortex. Nat Rev Neurosci 8:427–437.

Morante-Oria J, Carleton A, Ortino B, Kremer EJ, Fairén A, Lledo PM (2003) Subpallial origin of a population of projecting pioneer neurons during corticogenesis. Proc Natl Acad Sci U S A 100:12468–12473.

Murata T, Furushima K, Hirano M, Kiyonari H, Nakamura M, Suda Y, Aizawa S (2004) ang is a novel gene expressed in early neuroectoderm, but its null mutant exhibits no obvious phenotype. Gene Expr Patterns 5:171–178.

Muzio L, Mallamaci A (2005) Foxg1 confines Cajal-Retzius neuronogenesis and hippocampal morphogenesis to the dorsomedial pallium. J Neurosci 25:4435–4441.

Packer AN, Xing Y, Harper SQ, Jones L, Davidson BL (2008) The bifunctional microRNA miR-9/miR-9* regulates REST and CoREST and is downregulated in Huntington's disease. J Neurosci 28:14341–14346.

Roy K, Kuznicki K, Wu Q, Sun Z, Bock D, Schutz G, Vranich N, Monaghan AP (2004) The Tlx gene regulates the timing of neurogenesis in the cortex. J Neurosci 24:8333–8345.

Sakakibara S, Imai T, Hamaguchi K, Okabe M, Aruga J, Nakajima K, Yasutomi D, Nagata T, Kurihara Y, Uesugi S, Miyata T, Ogawa M, Mikoshiba K, Okano H (1996) Mouse-Musashi-1, a neural RNA-binding protein highly enriched in the mammalian CNS stem cell. Dev Biol 176:230–242.

Schuurmans C, Armant O, Nieto M, Stenman JM, Britz O, Klenin N, Brown C, Langevin LM, Seibt J, Tang H, Cunningham JM, Dyck R, Walsh C, Campbell K, Polleux F, Guillemot F (2004) Sequential phases of cortical specification involve Neurogenin-dependent and -independent pathways. EMBO J 23:2892–2902.

Shibata M, Kurokawa D, Nakao H, Ohmura T, Aizawa S (2008) MicroRNA-9 modulates Cajal-Retzius cell differentiation by suppressing Foxg1 expression in mouse medial pallium. J Neurosci 28:10415–10421.

Siegenthaler JA, Tremper-Wells BA, Miller MW (2008) Foxg1 haploinsufficiency reduces the population of cortical intermediate progenitor cells: effect of increased p21 expression. Cereb Cortex 18:1865–1875.

Simpson TI, Pratt T, Mason JO, Price DJ (2009) Normal ventral telencephalic expression of Pax6 is required for normal development of thalamocortical axons in embryonic mice. Neural Dev 4:19.

Stenman J, Toresson H, Campbell K (2003a) Identification of two distinct progenitor populations in the lateral ganglionic eminence: implications for striatal and olfactory bulb neurogenesis. J Neurosci 23:167–174.

Stenman J, Yu RT, Evans RM, Campbell K (2003b) Tlx and Pax6 co-operate genetically to establish the pallio-subpallial boundary in the embryonic mouse telencephalon. Development 130:1113–1122.

Stenman JM, Wang B, Campbell K (2003c) Tlx controls proliferation and patterning of lateral telencephalic progenitor domains. J Neurosci 23:10568–10576.

Sussel L, Marin O, Kimura S, Rubenstein JL (1999) Loss of Nkx2.1 homeobox gene function results in a ventral to dorsal molecular respecification within the basal telencephalon: evidence for a transformation of the pallidum into the striatum. Development 126:3359–3370.

Tamura S, Morikawa Y, Iwanishi H, Hisaoka T, Senba E (2004) Foxp1 gene expression in projection neurons of the mouse striatum. Neuroscience 124:261–267.

Tarabykin V, Stoykova A, Usman N, Gruss P (2001) Cortical upper layer neurons derive from the subventricular zone as indicated by Svet1 gene expression. Development 128:1983–1993.

Toresson H, Potter SS, Campbell K (2000) Genetic control of dorsal-ventral identity in the telencephalon: opposing roles for Pax6 and Gsh2. Development 127:4361–4371.

Tuoc TC, Stoykova A (2008) Er81 is a downstream target of Pax6 in cortical progenitors. BMC Dev Biol 8:23.

Vasudevan S, Steitz JA (2007) AU-rich-element-mediated upregulation of translation by FXR1 and Argonaute 2. Cell 128:1105–1118.

Vasudevan S, Tong Y, Steitz JA (2007) Switching from repression to activation: microRNAs can up-regulate translation. Science 318:1931–1934.

Wakiyama M, Takimoto K, Ohara O, Yokoyama S (2007) Let-7 microRNA-mediated mRNA deadenylation and translational repression in a mammalian cell-free system. Genes Dev 21:1857–1862.

Watanabe K, Kamiya D, Nishiyama A, Katayama T, Nozaki S, Kawasaki H, Watanabe Y, Mizuseki K, Sasai Y (2005) Directed differentiation of telencephalic precursors from embryonic stem cells. Nat Neurosci 8:288–296.

Yagi T, Tokunaga T, Furuta Y, Nada S, Yoshida M, Tsukada T, Saga Y, Takeda N, Ikawa Y, Aizawa S (1993) A novel ES cell line, TT2, with high germline-differentiating potency. Anal Biochem 214:70–76.

Yoo AS, Staahl BT, Chen L, Crabtree GR (2009) MicroRNA-mediated switching of chromatin-remodelling complexes in neural development. Nature 460:642–646.

Yoshida M, Assimacopoulos S, Jones KR, Grove EA (2006) Massive loss of Cajal-Retzius cells does not disrupt neocortical layer order. Development 133:537–545.

Yun K, Potter S, Rubenstein JL (2001) Gsh2 and Pax6 play complementary roles in dorsoventral patterning of the mammalian telencephalon. Development 128:193–205.

Yun K, Mantani A, Garel S, Rubenstein J, Israel MA (2004) Id4 regulates neural progenitor proliferation and differentiation in vivo. Development 131:5441–5448.

Zhao C, Sun G, Li S, Shi Y (2009) A feedback regulatory loop involving microRNA-9 and nuclear receptor TLX in neural stem cell fate determination. Nat Struct Mol Biol 16:365–371.

Zuccato C, Tartari M, Crotti A, Goffredo D, Valenza M, Conti L, Cataudella T, Leavitt BR, Hayden MR, Timmusk T, Rigamonti D, Cattaneo E (2003) Huntingtin interacts with REST/NRSF to modulate the transcription of NRSE-controlled neuronal genes. Nat Genet 35:76–83.